Imaging spectrometry of urban materials

Dar A. Roberts and Martin Herold

Department of Geography, EH3611, University of California, Santa Barbara, California, 93106

March 2004

Authors address:
Dar A. Roberts, Martin Herold
Department of Geography, EH3611
University of California
Santa Barbara, CA 93106
Ph 805-893-2276
Fax 805-893-3146
dar@geog.ucsb.edu
martin@geog.ucsb.edu

Reference:
Roberts, D. A. and M. Herold 2004. Imaging spectrometry of urban materials, in King, P., Ramsey, M.S. and G. Swayze, (eds.), Infrared Spectroscopy in Geochemistry, Exploration and Remote Sensing, Mineral Association of Canada, Short Course Series Volume 33, London, Ontario, pp. 155-181.

INTRODUCTION

Imaging spectrometers have considerable potential for urban applications. In this chapter we discuss how imaging spectrometry has been used for urban applications and provide an overview of instrumentation, sampling, spectroscopy, and analysis with a focus on urban materials. Case studies are presented for Santa Barbara California, in which we evaluate optimal wavelengths for urban mapping, and the World Trade Center, where imaging spectrometry was used to map environmental contaminants rapidly in response to the disaster.

There is a growing interest in the use of remote sensing in urban environments. Urban environments represent only a small percentage of land area, but they have become increasingly populated as greater numbers of individuals migrate from rural areas to cities, towns and suburbs. Globally, this trend has resulted in an increase in the urban population from approximately 2% in 1800 to estimates of over 50% by the turn of this century (Ben-Dor, 2001). Urban environments also have a growing impact on adjacent lands as sources of urban expansion into agricultural lands and native vegetation, sources of airborne and waterborne pollution, and net consumers of energy and resources (McNeill, 2000). There is a growing need for improved maps of urban surface materials, such as roof types for energy conservation and fire danger assessment (Woycheese *et al*. 1997; Medina, 2000), and impervious surfaces for improved estimation of flood potential and urban source pollution (Schueler, 1994; Ridd, 1995). The dynamic nature of urban environments necessitates technologies that are rapid, repeatable and provide large areal coverage at a reasonable cost, making remote sensing one of the most viable technologies.

Until recently, most analysis in urban areas has relied upon aerial photography as a data source. Urban environments are especially challenging because urban objects typically have a small spatial extent, making aerial photography well suited to these areas. Recent advances in spaceborne systems, such as IKONOS (www.spaceimaging.com) and Quickbird (www.digitalglobe.com) provide cost effective alternatives to aerial photography. For example, IKONOS provides 1 m panchromatic and 4 m multispectral data, thereby meeting the minimum spatial resolution of 5 m considered necessary for accurate spatial representation of urban materials such as buildings and roads (Woodcock and Strahler, 1987; Jensen and Cowen, 1999). Quickbird provides even finer spatial resolution, providing 0.61 m panchromatic and 2.44 m multispectral data. However, multispectral and panchromatic systems such as IKONOS do not provide sufficient spectral information (i.e. necessary wavelengths or enough bands sampled) needed to discriminate many urban materials (Herold *et al.* 2003). For example senesced (dead) grass and wood shingle can be definitively separated from bare soil, road surfaces and non-wooden roofs based on the expression of ligno-cellulose bands in the short-wave infrared (SWIR), yet these wavelengths are not sampled by either of these sensors.

Imaging spectrometers have sufficiently fine enough spectral sampling and sample enough wavelengths to address many of the weaknesses inherent in multispectral systems. Imaging spectrometers, such as the Airborne Visible/Infrared Imaging Spectrometer (AVIRIS; Table 1), consist of a large number of spectrally contiguous bands (Green *et al*. 1998). The intensity of electromagnetic radiation reflected by the surface at different wavelengths depends on the source function (the sun); the physical structure of the surface; the chemical constituents present; and the extent to which radiance is modified by the atmosphere (Schott, 1997). Imaging spectrometers, by sampling a large number of wavelengths, make it possible to better define each of these components, thereby improving the quality of retrieved surface reflectance and identifying the chemical and physical properties of materials within the field of view of the instrument (Green *et al*. 1998). Because many urban materials have unique chemical constituents, this offers the potential of improved mapping of urban land-cover through direct mapping of urban chemistry.

Table 1: Selection of airborne imaging spectrometers used in urban remote sensing and description of some key attributes. Sensors listed include AVIRIS (Airborne Visible Infrared Imaging Spectrometer, CASI (Compact Airborne Spectrographic Imager, DAIS7915 (Digital Airborne Imaging Spectrometer) HYDICE (Hyperspectral Digital Imagery Collection Experiment, HyMAP and MIVIS (Multispectral Infrared and Visible Imaging Spectrometer). Sources for AVIRIS, CASI and HYDICE include Green *et al.* (1998) and Kruse (1999). Information for the DAIS7915 can be located at http://www.op.dlr.de/dais/dais-scr.htm. Information on HyMAP was determined from http://www.intspec.com/Products/HyMapProd.htm.

Sensor	Spectral Range	FWHM	FOV	IFOV	GIFOV	Quantization
AVIRIS	370-2500 nm	10nm(nom)	32 deg	1mr	(20m/20km)	12 bit
	(224 bands)	(9.8nm samp)			(4m/4km)	
CASI	400-1000nm	2.2nm	37.8deg	1.25mr	(0.5m/0.4km)	12 bit
	(19 to 288 bands)	(1.9m samp)			(10m/8km)	
DAIS7915	450-2450nm	400-1000nm	51.2deg	3.3mr	(5m/1.5km)	15 bit
	(72 bands)	(15-30 nm, 32)			(20m/6km)	
	7 thermal	1500-1800nm				
		(45nm, 8)				
		2000-2500nm				
		(20nm, 32)				
HYDICE	400-2500nm	10nm (nom)	8.9 deg	0.5mr	(1m/2km)	12bit
	(210 bands)				(4m/8km)	
HyMAP	450-2500nm	15-22 nm	30-65deg	1-3mr	(1.5m/1.5km)	12-16bit
	(126 bands)	(VNIR 15-17nm)			(13.5m/4.5km)	
		(SWIR 17-22nm)				
MIVIS	430-830nm	20 nm	71 deg	2 mr	(5m/2.5km)	12 bit
	(20 bands)					
	1150-1550 nm	50 nm				
	(8 bands)					
	1985-2479 nm	8 nm				
	(64 bands)					
	10 thermal					

A number of researchers have begun to exploit the fine spectral structure of imaging spectrometry to map urban materials. Bianchi *et al.* (1996) used Multispectral Infrared and Visible Imaging Spectrometer (MIVIS) data to differentiate paving materials in Rome, Italy. Hepner *et al.* (1998) and Gamba and Houshmand (2001) used a combination of AVIRIS and Interferometric Synthetic Aperture Radar (IFSAR) to produce improved maps of three-dimensional urban structure in Los Angeles, California, USA. A similar study is described by McKeown *et al.* (1999), who used data acquired over Fort Hood, Texas, USA by the Hyperspectral Digital Imagery Collection Experiment (HYDICE; Table 1) to classify urban and natural materials and merged this map with stereo panchromatic imagery to map the three-dimensional structure of buildings. Ben-Dor *et al.* (2001) used a combination of an existing spectral library developed by Price

(1995) and Compact Airborne Spectral Imager (CASI; Table 1) data acquired over Tel Aviv, Israel, to develop an urban spectral library. They compared spectra of common urban materials, then used a subset of the library and a Mixture Tuned Matched Filter (MTMF: Boardman *et al*. 1995) to map materials within the CASI scene. In a review chapter on urban imaging spectrometry, Ben-Dor (2001) extended this work to include analysis of field spectra acquired using a full range Analytical Spectral Devices (ASD) spectrometer, noting that many urban materials sampled had unique "spectral fingerprints" associated with specific minerals within the materials. Roessner *et al*. (2001) used data acquired by the Digital Airborne Imaging Spectrometer (DAIS 7915; Table 1) to map urban materials in the city of Dresden, Germany. In this study, the authors used a maximum likelihood classifier (a classification procedure that assigns a spectrum to a specific class based on the probability that it is a member of that class) to produce a map of "pure" spectral endmembers, then used these spectra to seed a new algorithm that unmixed neighboring spectra as linear combinations of seed spectra. Heiden *et al.* (2001) used HyMap (Table 1) to produce a hierarchical thematic classification (see urban concepts below) of urban land cover types and materials and provided preliminary spectroscopic analysis of those targets. Herold *et al*. (2003) evaluated optimal wavelengths for mapping urban materials using AVIRIS data acquired over Santa Barbara, CA using the Bhattacharyya distance (Jimenez and Landgrebe, 1999) as a spectral separability metric. They compared AVIRIS to AVIRIS-simulated IKONOS and Landsat Thematic Mapper (TM) data to evaluate differences in map accuracy due to spectral sampling, finding that AVIRIS produced the highest map accuracies for many materials, most notably roofs. Recently, Clark *et al*. (2001) demonstrated the potential of an imaging spectrometer for disaster response. In this study, the authors used high spatial resolution AVIRIS data acquired over the World Trade Center to map thermal sources, asbestiform minerals and dust and debris from the collapse, producing maps of environmental contaminants that are difficult to produce cost effectively in any other way.

Whereas current spaceborne systems, such as Hyperion on EO-1 (Ungar *et al*. 2003) lack sufficiently small-scale (fine) spatial resolution for most urban applications, initial studies with airborne systems provide a glimpse of the potential power of combining fine spatial resolution with fine spectral sampling. The increasing availability of airborne imaging spectrometer data, and potential for finer spatial resolution spaceborne data in the future suggest that this technology will continue to grow in importance. In this chapter we provide an overview of some of the techniques used to measure spectra of urban materials, discuss unique spectral properties of these materials, spectral analysis techniques commonly employed and conclude with some examples from our own work.

IMPORTANT CONCEPTS

Radiometry, imaging and imaging geometry

Imaging spectrometers measure electromagnetic radiation reflected or emitted from the atmosphere or surfaces. A majority of imaging spectrometers deployed for terrestrial applications sample reflected and emitted wavelength ranges from the ultra-violet (UV) to the Near- Infrared (NIR), covering a spectral range from 350 to 2500 nm. In this chapter, we will focus on the visible near IR (VNIR, or 400-1000 nm; Chapter 1) and the short wave infrared (SWIR, 1000-2500 nm; Chapter 1), which is part of the near-IR (NIR). The most common energy source for radiation in the visible and NIR is the sun, although active sensors such as Light Detection and Ranging (LIDAR) also operate in this spectral region. The NIR infrared radiation is generally detected by silicon-based detectors and the SWIR radiation is detected by indium antimonide (InSb) or lead sulfide (PbS) detectors (e.g., Schott, 1997; Chapter 2).

The most useful way of reporting spectral values is in units of reflectance. Reflectance can be defined as the ratio of the measured radiance from an object divided by the radiance reflected by a near-perfect reflector (e.g., pressed halon). In this manner, reflectance spectra are standardized and thus the spectrum of an unknown material can be compared to a known material while removing other factors that modify reflected radiation, such as the light source, illumination geometry or effects of external energy sources such as scattered radiation. Reflectance can be expressed in a variety of ways depending upon the nature and geometry of the incoming and reflected radiation and the type of spectrometer. The two most common types of reflectance used in remote sensing include directional-hemispherical reflectance and bi-directional reflectance. Directional-hemispherical reflectance is typically measured in the laboratory using a collimated beam as the directional source, and an integrating sphere to capture reflected radiation at all possible view geometries. Bidirectional reflectance is typically measured in the field or by most imaging spectrometers. In this case, incident energy and reflected energy are measured from a specific set of incident and view angles. A common geometry used in the field, for example, is to orient the sensor normal to the surface (nadir viewing), with the sun positioned at a specific zenith and azimuth angle depending on geographic location, time of day and date. In this chapter, all spectra are bi-directional with units of reflectance.

Remote sensing systems do not measure reflectance. Rather, they provide some measure of the amount of radiation reflected by an object, which varies depending upon the sensitivity of the instrument, wavelengths sampled, lighting geometry and atmospheric conditions. The remote sensing signal also depends on the quantization of the recorded signal. Quantization describes the number of bits used to store a number. For example; 8 bit quantization stores 256 values, and 12 bit stores 4096. Different remote sensing platforms have different inherent quantization (Table 1).

Raw data values from an instrument are typically called Digital Numbers (DNs). Reflectance can be derived from DNs provided that light reflected by an object is standardized to light reflected off of a material of known reflectance under similar lighting conditions. A common field standard is Spectralon (Labsphere, New Hampshire), consisting of pressed halon powder. For laboratory or field instruments, the process of converting DNs to reflectance can either be performed automatically by the instrument once a reflectance standard is acquired, or calculated later from DNs. The same process, however, cannot be as easily implemented using imaging spectrometry data. In this case, a key intermediate step is the process of radiometric calibration, in which DNs recorded by the instrument, are converted to units of spectral radiance, L_λ, through a series of wavelength dependent instrumental gains and offsets ($L_\lambda = Gain_\lambda * DN_\lambda + offset_\lambda$). Instrumental gains and offsets are typically established in the laboratory using a calibrated light source and integrating sphere (prelaunch or preflight gains and offsets). However, instrumental performance can also be monitored in flight using on-board light sources and the instrumental gains and offsets can be adjusted after a flight has occurred using ground targets (e.g. Green and Pavri, 2002).

Units of spectral radiance vary considerably between sensors (e.g., Table 1). For example, typical units reported by AVIRIS are $\mu W cm^{-2} nm^{-1} sr^{-1}$. The process of radiometric calibration is particularly important in the field of imaging spectrometry, because it is a fundamental requirement for atmospheric correction and reflectance retrieval.

Other important components of calibration include spectral calibration, reporting the band center and spectral response for each detector. The spectral response for most imaging spectrometers is considered to have a Gaussian shape, and is typically described by the Full-Width-Half-Maximum of the band (FWHM:

equal to the spectral width of the response function at half the peak response; Fig. 1). The AVIRIS sensor, for example, has a nominal FWHM of 10 nm and spectral calibration of 0.5 nm or better with an absolute radiometric calibration of 96% averaged across the spectrum (Green *et al.* 2002). The FWHM of a system is commonly referred to as its spectral resolution. However, spectral resolution is more properly defined as the minimum spectral separation required to discriminate two spectral features, and thus can be less than or greater than the FWHM. For example, the kaolinite doublet is clearly discernable with a FWHM of 20 nm or finer, but is no longer evident at a FWHM of 50 or 100 nm (Fig. 1b). Spectral resolution (the ability to resolve a spectral feature) will depend on the FWHM, wavelength location of band centers and sampling interval (Fig. 1; Swayze *et al*., 2003)

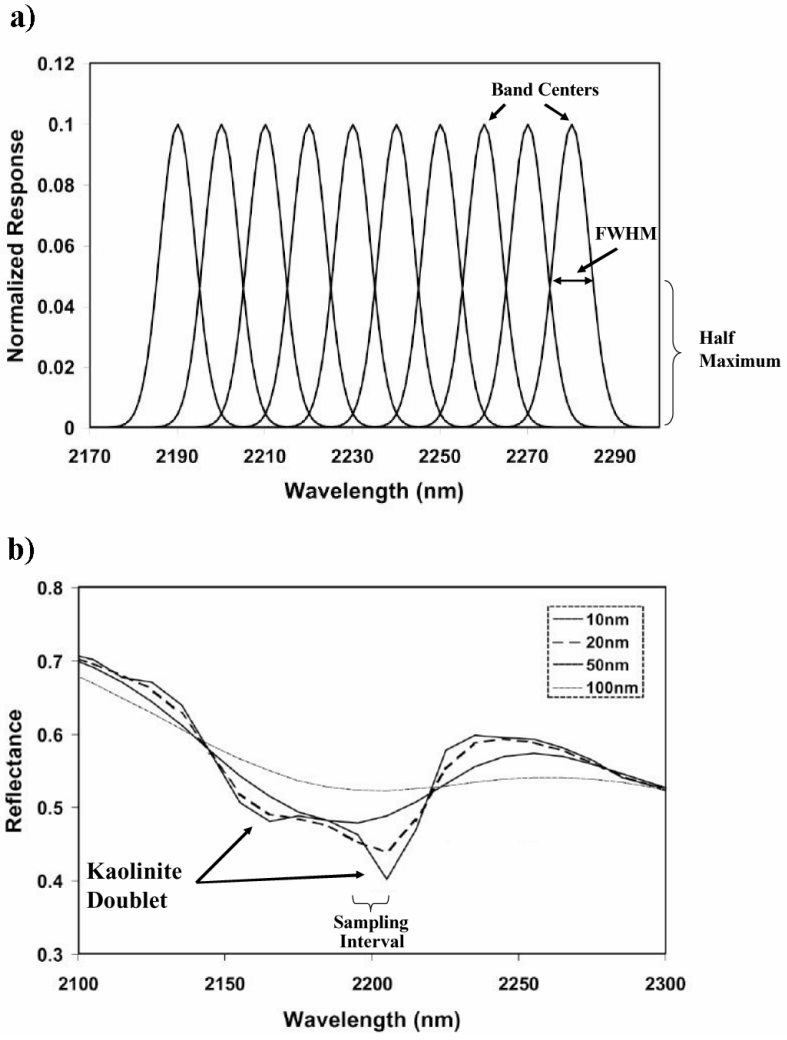

Figure 1) (a) Plot showing the FWHM and band centers for 10 wavelengths sampled between 2190 and 2280 nm with a 10 nm FWHM. (b) illustrates the impact of FWHM on spectral resolution. In this example, the kaolinite doublet is evident at a FWHM of 10 and 20 nm, but is not evident at a FWHM of 50 and 100 nm.

Several important aspects of imaging also must be taken into consideration. Imaging spectrometers differ from laboratory or field-based spectrometers in that they create an image of spectra. Important spatial

components of an imaging spectrometer include the Field of View (FOV, or cross-track width; Fig. 2) and the Instantaneous Field of View (IFOV). The FOV describes the angular width imaged by the sensor in the cross track direction and is typically reported in degrees or kilometers (Fig. 2). For example, AVIRIS when deployed on the ER-2 measures 614 cross track elements, equal to a 32 degree FOV and a nominal swath width of 11 km (Green *et al*. 1998). Cross-track spectra are most typically acquired using two imaging strategies, pushbroom systems and whiskbroom systems. In a pushbroom system, each cross-track element is sampled by a different set of detectors, thus reducing the need for moving parts and increasing the time a set of detectors can image the same piece of ground. In a whiskbroom sensor, each cross track element is sampled by the same set of detectors which image different portions of the FOV through the use of scanning foreoptics or rotating mirrors. Whiskbroom sensors are easier to radiometrically calibrate than pushbroom sensors, but also require more moving parts and have less time to image the same area (thus potentially impacting SNR). A common artifact in pushbroom sensors is vertical striping in images, due to cross track differences in the radiometric calibration of detectors. Examples of pushbroom systems include CASI and HYDICE while AVIRIS, HyMAP and the DAIS7915 are whiskbroom systems (Table 1).

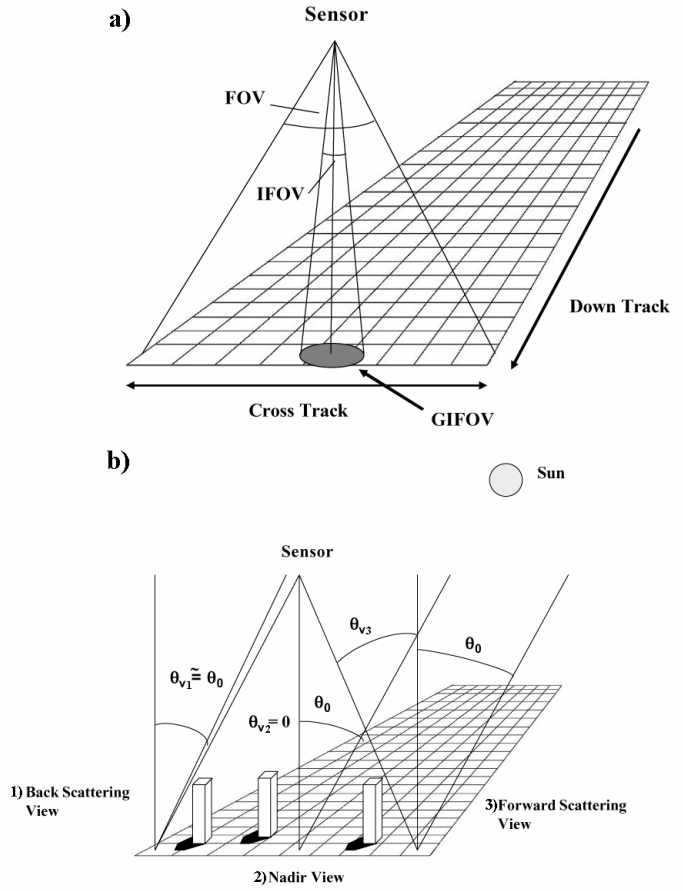

Figure 2) (a) Typical imaging geometry including the sensor, FOV, IFOV, GIFOV, across track and along track sampling. (b) Typical illumination geometry, showing the solar zenith, θ_0, and view zenith, θ_v, as they vary across the image from a forward scattering (3), to nadir (2) and backscattering (1) geometry. Tall buildings will be darkest in the forward scattering view direction because the sensor is imaging shadows cast by the buildings.

The IFOV describes the angle subtended by a single detector element and is typically reported in milliradians. When the IFOV is multiplied by sensor height, this is called the Ground Instantaneous Field of View (GIFOV; Fig. 2). The IFOV of AVIRIS is 1 milliradian, producing a GIFOV of 20 m from a height of 20 km. For urban remote sensing probably the most important sensor attribute to consider is the GIFOV. As is true for spectral resolution, spatial resolution is commonly used synonymously with the GIFOV, but is more properly defined as the minimum distance between two objects required to discriminate them. As such, spatial resolution varies depending upon atmospheric conditions and the contrast between two objects on the ground.

Special consideration must be given to the interplay between the bidirectional reflectance of a surface, and imaging and illumination geometry (Fig. 2b). The manner in which reflectance of an object varies depending on solar and view zenith can be described as a function called the Bidirectional Reflectance Distribution Function (BRDF; Schott, 1997). Surfaces can be categorized as Lambertian (scatters equally in all directions), backscattering (preferentially scatters light back to the source), forward scattering (preferentially scatters light away from the source), specular (mirror) or some combination of these. Most rough surfaces, such as shrubs, trees and buildings, backscatter radiation, whereas smooth surfaces like water reflect radiation in a specular manner. Dry beach sands and sidewalks scatter radiation in a near Lambertian manner. Depending on the orientation of a flight line and the solar azimuth, one flank of the imaging swath may represent either a forward or backscattering view geometry. This becomes important because viewing geometry can modify the overall brightness and spectral properties of a surface. For example, the lighting geometry shown in Figure 2b will result in a strong gradient from the right to left, with the lowest radiance in the forward scattering view (where the sensor is imaging shadows cast by buildings) and highest radiance in the backscattering view (where the shadows are partly blocked by the buildings). The BRDF of some materials varies spectrally. For example, vegetation is a backscatterer in the visible part of the spectrum, but more lambertian in the NIR (Deering, 1989). The spectral dependence of the BRDF for most urban materials is poorly known.

Viewing geometry can be particularly problematic when mosaicking overlapping flight lines. The most ideal flight geometry is to have the aircraft flying either towards or away from the sun, because this gives each side of the swath the same viewing geometry. However, this ideal is not always achievable. For example, in our own work in Santa Barbara, California, USA, the east-west orientation of the Santa Ynez range forces east-west flights. As a result, two mosaicked east-west AVIRIS flights can produce differences of up to 32 degrees in view zenith in the overlap region.

Urban terminology

Additional important concepts include the nature of applications in urban areas. Common terminology in urban remote sensing distinguishes between land-cover (the material composition) and land-use (how the land is used). Remote sensing allows us to map land-cover, but only infer land-use. Land-cover categories are typically placed in a hierarchical classification scheme developed by Anderson *et al.* (1976), in which broad land-cover classes are considered Level 1 and only require relative coarse spatial resolutions (20-100 m). Level 4 requires sub-meter resolution, and involves very detailed use information (Jensen and Cowen, 1999). As an example, the designation urban, or "built-up" refers to an Anderson Level 1 class, subdivision between residential and commercial uses would be Level 2, a distinction between single and multifamily residential would occur at Level 3 and Level 4 might entail separating retail from office use for a commercial class. The hierarchical scheme developed by Anderson et al (1996) is commonly modified to suit the needs of an application. Herold *et al.* (2003) adhered to Anderson Levels 1 and 2 in their study, but

modified Level 3 to include materials (i.e., wood shingle versus composite shingle) and Level 4 as a subdivision within a type of material (i.e., black composite shingle).

Another powerful classification scheme proposed for urban areas is the VIS model (Vegetation-Impervious Surface-Soil; Ridd, 1995), in which roofs and road surfaces would be categorized as impervious surfaces, whereas an open lot or park might be vegetation or bare soil. Imaging spectrometry has its greatest potential in identifying materials (Level 3 or 4) and improving separation at Level 2.

EQUIPMENT AND SAMPLING

Overview

The quality of spectral data is highly dependent upon the quality of the instrumentation. Important considerations when evaluating an instrument include spatial, spectral, and stability concerns. Spatial considerations include GIFOV as discussed previously. Spectral considerations include the wavelength range sampled, number of wavelengths sampled within this range and the FWHM (Table 1). Additional considerations include the stability of spectral calibration and potential of artifacts, such as second-order contamination or out of band transmission , both of which entail measuring radiation from outside of the wavelength region of interest. For example, the use of a grating to disperse light can lead to second-order contamination, whereas the FWHM produced by a prism can vary as a function of the wavelength sampled (a slit can be used to compensate for wider dispersion). Many of these factors vary depending upon the method of light dispersal and the arrangement of detector arrays within the instrument. Precise knowledge of the spectral properties of an instrument is critical if spectra are to be convolved to a variety of sensors with differing spectral response functions.

Radiometric considerations include radiometric stability, quantization and signal to noise ratio (SNR: alternatively instrumental noise can be expressed as a Noise Equivalent Delta Radiance, or NEDL). An ideal instrument is radiometrically stable, and has sufficiently high enough SNR, and quantization to discriminate two materials based on subtle differences in reflectance (Swayze *et al*., 2003). AVIRIS, for example, uses 12 bit quantization and had a SNR that exceeded 1000:1 in the visible, and approached 500:1 at 2200 nm in 2001 (Green *et al*. 2002).

Instrumentation

Spectra are typically acquired at three scales, in the laboratory from destructive samples (i.e., leaves harvested in the field and brought into the laboratory), in the field (termed in-situ by Ben-Dor, 2001) or from an imaging platform. Because laboratory-based instruments have been covered in detail in other chapters, little will be said here. Typically laboratory based measurements are made over a fairly small sample, with a field of view on the order of 0.01-2 cm^2. As stated previously, laboratory-based instruments typically measure directional-hemispherical reflectance. These instruments have the advantage of providing controlled conditions and the highest quality reflectance, but also require the transport of surfaces into the laboratory environment. In many cases, this is infeasible.

A number of high quality field instruments are available. In our own research, we have used the Spectron-SE590, ASD Personal Spectrometer II, GER Field Spectrometer Mark IV, and ASD full range instrument. In addition to considerations of instrumental performance, other factors become important in the field, such as the weight of the instrument, its durability, scan time, software and number of documented artifacts. In this chapter, all of the field-based spectra were acquired using an ASD full range instrument. This instrument samples between approximately 350 and 2500 nm at a spectral sampling interval of 1.4 nm in

the VNIR with a FWHM of 3-4 nm and interval of 2.2 nm in the SWIR with a 10-12 nm FWHM. Spectra can be collected over a range of IFOVs, controlled by the foreoptics (a device that restricts the IFOV), which range from 1 (highly restricted) to 25 degrees (no foreoptics). Output spectra are resampled to a 1 nm interval. Scan times are typically rapid, allowing spectral averaging of 10 or more spectra in a few seconds. Spectra are sampled using a grating, a silicon-based detector array for 350-1000 nm and two InGaAs SWIR detectors that sample from 1000 to 2500 nm (http://www.asdi.com). The SNR of the instrument varies depending on the illumination source and wavelength sampled, with the lowest SNR found within strong water vapor absorption regions (1400 and 1900 nm), at the longest wavelengths (2500 nm) and at the transition zone between the VNIR and SWIR1 detectors at 1000 nm. A contact probe is also available for small samples, which avoids the need of solar illumination through an internal light source. Although models vary, the instrument is generally portable with high performance.

Sampling strategy

A key consideration in the field is sampling strategy. Sampling choices include the choice of foreoptics, height above the target, frequency that spectra are standardized, time of day, acceptable atmospheric conditions and number of samples for each target. Ideally spectra should be acquired when the solar zenith is lowest, typically within +/- 2 hours of solar noon under clear sky conditions, although the range of acceptable times will depend on latitude, time of year and the frequency at which standards are measured. For example, in Santa Barbara (34N latitude), if standards are acquired every five minutes, acceptable spectra can be acquired within +/-3 hours of solar noon in July, but only within +/- 1.5 hours of solar noon in January (this assumes a 5% change in radiance measured between standards is acceptable). At higher latitudes, the acceptable range will be far shorter during the winter, but may be greater during the summer. Reflectance standards should also be acquired under the same illumination conditions as the surface to avoid the impact of side scattered light. For example, if a target is measured in close proximity to a tree, but the standard is measured away from the tree, the lighting environment of the target will include higher levels of NIR than the standard, thus producing an anomalous spectrum (side scattered radiation is also called the adjacency effect). Adjacency effects will be most significant in rough urban environments.
In urban environments sampling strategies can be complicated. The simplest sampling problem involves horizontal surfaces, such as roads, parking lots, sidewalks or lawns. In this instance, the height of the instrument and number of measurements required will depend on the variability of the surface and the objectives of the measurements. For example, a relatively uniform, newly surfaced parking lot may require very few measurements to capture its spectrum. In contrast, if the objective is to quantify very fine scale variability, such as the impact of cracks on a road surface, many measurements may be required with the instrument positioned close to the surface (a few tens of cm). In our case, we typically sample road surfaces along transects at a fixed interval with the instrument positioned one meter above the surface. Transects range in length from less than 20 m to up to 100 m depending on the extent of the surface. Standards are acquired approximately every five minutes to avoid major changes in lighting between measurements. Because considerable variation exists in roads due to aging, building material and wear, a comprehensive library requires representatives from each of these categories.

Vertical structures and non-horizontal surfaces, which are common in urban environments, provide considerably greater challenges. For example, to sample roof spectra the instrument may have to be transported to the roof. Instrument height will vary depending upon the degree of purity desired. If the objective is to sample one shingle, the height and foreoptic must be selected to restrict the field of view to the small illuminated portion of the shingle. If the objective is to capture multiple shingles, or shadows cast by a shingle, a larger foreoptic or higher sensor height must be selected. To capture variability within a single roof, multiple spectra may be required on the same roof aspect, or spectra may be required on

different aspects on the same roof. In our own work, spectra were typically acquired from multiple shingles on at least four different roof aspects. Because of the non-lambertian behavior of most of these structures, reflectance will vary throughout the day, even if the aspect is constant. Vertical surfaces, such as plants add additional complications, such as variable heights of surfaces and considerable variation in shadowing, leaf orientations, branches etc. In order to characterize this variability, we typically sample multiple spectra within a single plant, and multiple plants within a species (Roberts *et al*. 2003).

Figure 3 illustrates a typical example of collecting spectra of urban materials using a field spectrometer. In this example, a researcher is collecting spectra of a concrete surface located within a parking lot in Goleta, California in late May, 2001. Spectra were sampled along a transect at fixed intervals of a few meters. At each interval five replicates were collected, each replicate consisting of the average of 10 spectra measured by the instrument. Spectra were originally collected in raw DN mode, standardized with a Spectralon panel (acquired at the start and end of the transect), then later processed to reflectance.

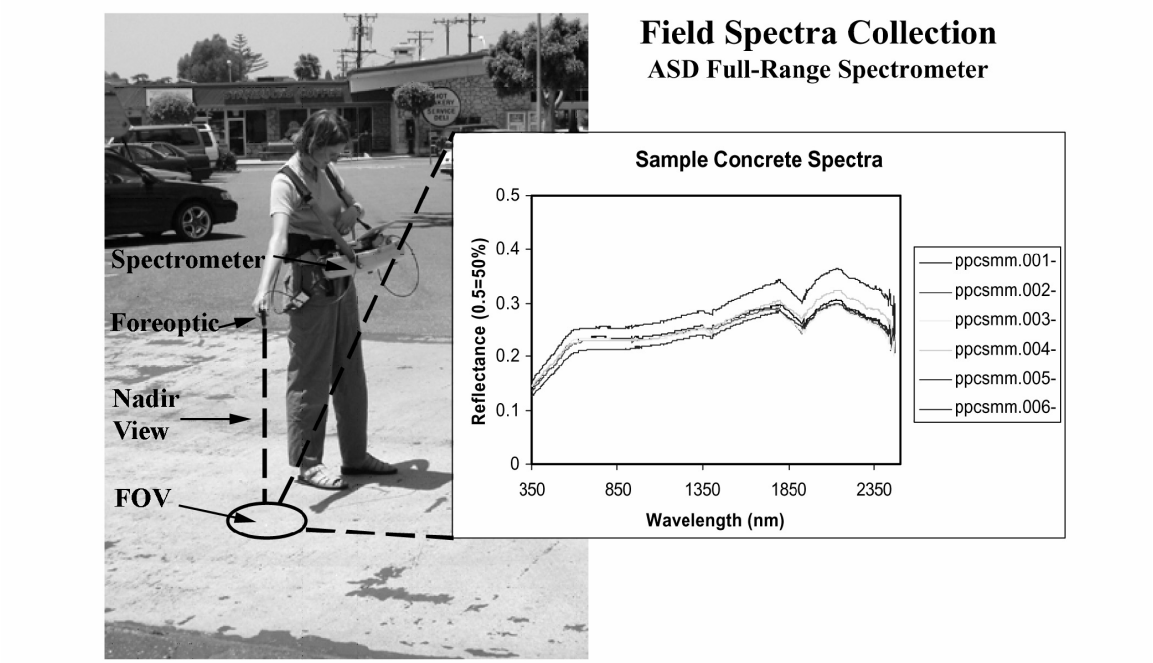

Figure 3) A researcher collecting spectra of a concrete surface located in a parking lot west of Fairview, Goleta California. Spectra measured along a transect over the surface are shown to the right.

If possible, photographs should be acquired and detailed metadata recorded for as many spectra as is feasible (Fig. 4). Metadata recorded for most of our urban spectra included CCD images of surfaces, GPS location, a short description of the material, time of day, a quality assessment of spectra and any additional descriptive terms such as age of surface, heterogeneity, surface quality etc (Fig. 4). In this manner, detailed variation within the FOV of the instrument and specific surface properties are described photographically, while other important descriptive information is also recorded.

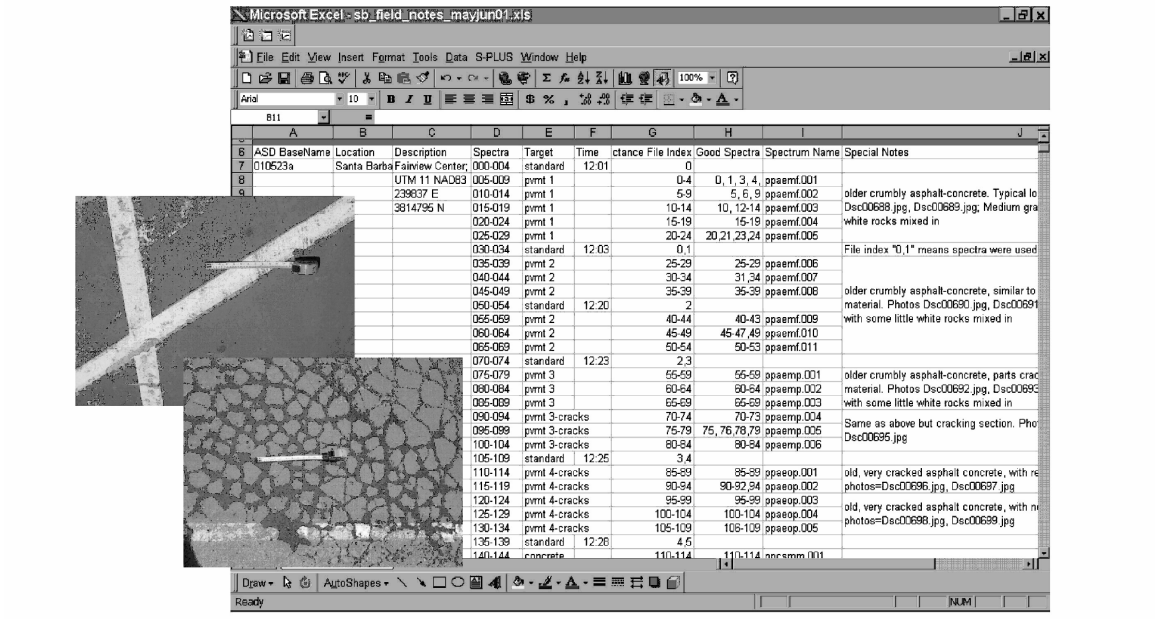

Figure 4) Typical metadata and digital images collected during the development of the Santa Barbara urban spectral library.

Low-flying airborne platforms offer the potential of acquiring a large number of spectra over many targets in very little time. Ben-Dor *et al.* (2001) and Herold *et al*. (2003) describe strategies in which high-resolution imaging spectrometry data were used to build a spectral library of urban materials. A growing number of imaging spectrometers are available that provide sufficiently fine spatial resolution to build a spectral library and map urban materials (Table 1). In this table, we focus only on imaging spectrometers that have recently been used to map urban areas. Key attributes listed in the table include the wavelength range, number of bands, FWHM, FOV, IFOV, GIFOV and quantization. We report nominal values of FWHM and, where it is reported, average spectral sampling intervals (in nm). The FOV, IFOV, FWHM and wavelengths ranges are typically fixed by the spectrometer. In contrast, GIFOV varies considerably depending on aircraft height, ranging from a fine GIFOV of 0.5 m, sampled by CASI deployed on a helicopter, to 20 m for DAIS7915 deployed at an altitude of 6 km. In some instances, instruments are programmable. CASI, for example, can be programmed in mapping mode, providing 19 bands for a cross track image of 512 elements, or spectral mode in which 288 bands are sampled at fixed spacings across the swath. Most urban studies using imaging spectrometers have utilized low altitude platforms (e.g., Mckeown *et al*. 1999; Ben-Dor *et al*. 2001; Roessner *et al*. 2001; Herold *et al*. 2003) and GIFOVs on the order of 4 m or less. The FWHM and spectral sampling are also potentially important. Although few studies have evaluated the importance of spectral information for urban areas (see Herold *et al*. 2003 for an exception), material specific vibrational absorptions in the SWIR suggest that sensors such as CASI, which lack these wavelengths, may have difficulty in discriminating certain types of materials. However, many unique urban spectral features are still present in the visible portions of the spectrum (Ben-Dor, 2001; Herold *et al*. 2003; Swayze *et al*. 2003;) suggesting that imaging spectrometers that do not sample the SWIR, are still likely to be able to map a large diversity of materials in these environments. A more detailed review of most of the sensors and several more is provided by Kruse (1999).

Key considerations when using imaging spectrometry data include time of acquisition, orientation of the flight, atmospheric conditions, GIFOV and quality of georeferencing. As stated previously, flight orientation can also be critical. Flights that parallel the solar azimuth are preferred over flights that are perpendicular to the azimuth. When possible, field spectra should be acquired either close to the time of acquisition, or from temporally invariant targets for use in reflectance retrieval (Clark *et al*., 2002).

IDENTIFICATION OF PEAKS AND/OR QUALITATIVE ANALYSIS AND/OR SPECTRAL MATCHING TECHNIQUES

The spectra of urban materials are dominated by the same electronic and vibrational absorption processes that create the spectra of plants and minerals. However, because of the way urban materials are altered by manufacturing processes and the way they are combined, it is not always easy to identify a specific absorption feature, and relate it to a diagnostic absorption process. Furthermore, man-made materials generate additional chemical absorptions which are not readily found in natural materials. A good example is paint, which has no analog in the natural world. Finally, urban spectra are further modified by processes that alter the original material. For example, road surfaces and roofs change with aging, leading to changes in their spectra. Urban materials can also be altered by coatings such as algae, dirt, dust or rubber tire marks found on roads, bridges and road paints. Remote sensing images of urban areas commonly contain pixels that represent a mixed spectral signature.

The same general principles developed for mineral spectroscopy can be applied the interpretation of urban spectra. Electronic absorption processes are typically high energy, involving the transition of an electron from one valence state to another, or to a non-valence state such as a conduction band (Clark, 1999). The high energy of these interactions typically results in strong absorptions in the UV, visible and shorter wavelength portions of the SWIR. Typical band shapes are broad, such as chlorophyll bands centered at 450 and 680 nm or iron-oxide absorptions, centered at 880 nm. The former are due to conjugate bands in the chlorophyll molecule, and the latter are due to crystal field absorptions in iron-oxides (e.g., Clark, 1999).

Vibrational bands represent lower energy absorptions occurring when the energy of photons matches the frequency of vibration of molecular bonds ($Q=h\nu$, where Q is radiant energy, in Joules, h is Planck's constant, and ν is frequency). Examples of molecules that produce vibrational absorptions within the NIR include water, hydroxyl, carbon dioxide, carbonates, sulfates and methane (Clark, 1999). In many instances, the fundamental frequency of absorption is beyond 2500 nm, but overtones and combinations can produce higher frequency vibrations that produce absorptions within the SWIR. Vibrational bands occur at longer wavelengths than those due to electronic processes, and typically are less broad. For a more detailed discussion of spectroscopy and absorption processes, see Clark, 1999.

Urban materials commonly vary regionally due to local resources, such as the availability of marble, wood or limestone for construction or due to local customs which can vary the ingredients used in roof materials, tile, brick and concrete aggregates (Ben-Dor, 2001; Hepner, Verbal commun. 2004). For example, many of the spectra published by Ben-Dor (2001) for Tel Aviv, show prominent calcium carbonate absorptions that are nearly lacking in the Santa Barbara area. The potential impacts of local customs and source materials should be taken into account when developing regional spectral libraries and caution should be used when exporting a spectral library from one part of the world to another.

Example spectra from the Santa Barbara area illustrate electronic and vibrational absorptions (Figs. 5a-d and 6a-d). Unless otherwise stated, spectra were acquired within +/- 2 hours of solar noon from heights of 1 m or less above the surface. Spectra were typically collected by setting the ASD in raw DN mode, setting the instrument to average 10 spectra per measurement, and collecting 5 replicates per sample. Each replicate was standardized to reflectance using a Spectralon standard acquired within 5 minutes of the sample. Reflectance spectra for each replicate were then assessed for quality, and averaged to produce a single spectrum for each sample. Figures 5a-d show a selection of roofing materials, bare soil, non-photosynthetic vegetation (NPV: Roberts *et al*. 1993) and residential grass. Figure 3a shows six types of composite shingle with relatively low reflectance spectra (5 to 20%) that in many cases are nearly featureless. Exceptions are the dark grey tile (1), which shows a minor peak in green wavelengths (520 nm); and the light tan/orange tiles (3) and light grey shingle (4), which show evidence of the presence of carbonates in the mixture (~2330 nm). Figure 5b shows a selection of wood shingle. All of these spectra show vibrational bands centered around 2100 and 2300 nm due to the presence of lignin and cellulose. Reflectance differences between spectra are in part due to different ages and degrees of weathering. Three wood shingle spectra show subtle absorptions due to the presence of chlorophyll in moss, algae and lichens. Similar findings are reported by Ben-Dor (2001), who points out the important role of coatings on modifying urban spectra. Ligno-cellulose bands are particularly important in helping distinguish wood shingle from bare soil or other roof types.

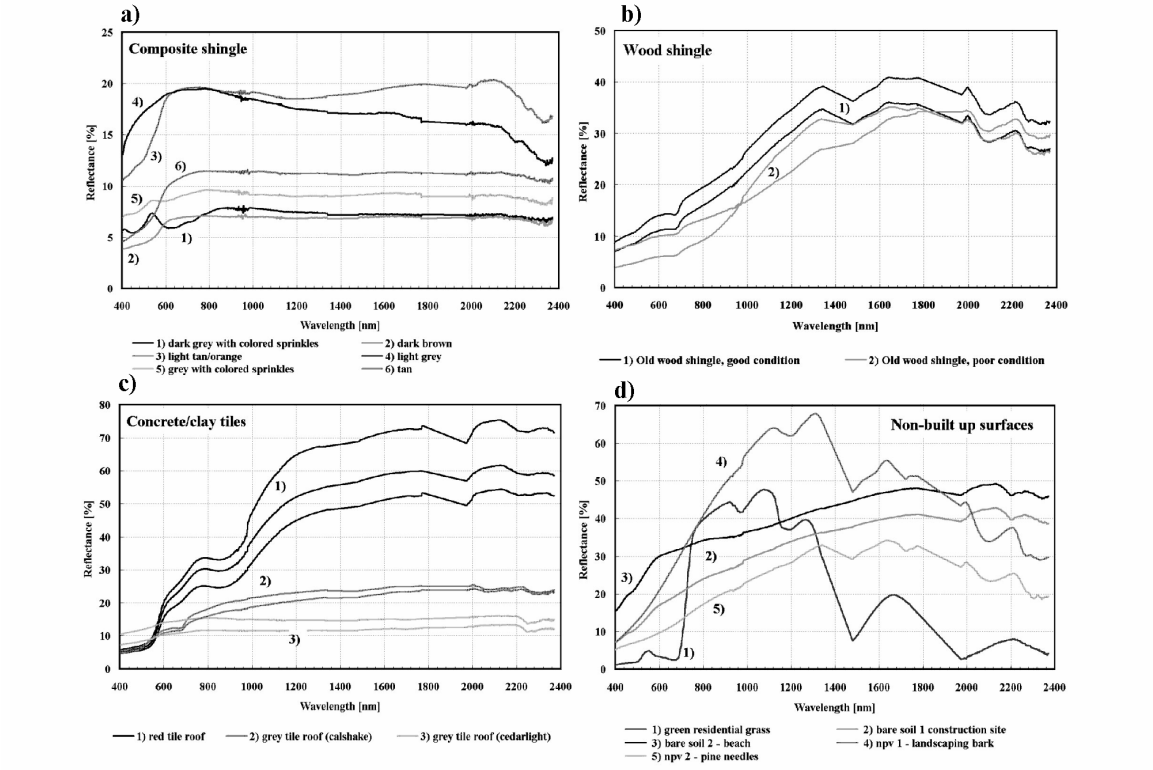

Figure 5) Spectra of typical roof materials and non built-up cover types from the Santa Barbara ASD urban spectral library. (a) shows typical composite shingle spectra, (b) shows concrete tiles, (c) wood shingle and (d) a variety of non-built up surfaces. Note: The small-scale variations at ~950 nm are an artifact of the field spectrometer and represent the area of transition/overlap between the sensor materials. Other sensor induced spectral variations relate to the "noisy" signal in the SWIR II region above 2300 nm. These artifacts are present in all spectra and appear strongly in low reflectance targets. The major water vapor absorption bands are interpolated. Note the different scales in the y-axis.

Figure 5c shows 7 spectra of red tile (1), calshake (2: a synthetic inorganic substitute for wood shingle), and cedarlite (3:a concrete substitute for wood shingle). Strong visible light absorption in red tile and absorptions in the NIR represent iron-oxide absorption features centered at 520 nm, 670 nm and 870 nm. Liquid water and hydroxyl absorptions, typically found in clays, are lacking in fired brick and the reflectance is higher towards longer wavelengths due to the loss of water in the production firing process (Heiden *et al*. 2001). A comparison of red tile from Santa Barbara, to spectra published by Ben Dor (2001), demonstrates remarkable similarities in the composition of red brick in Israel and Santa Barbara. Synthetic wood shingles (consisting of concrete or cement), although resembling wood shingle in the visible portions of the spectrum, are nearly featureless in the SWIR.

Figure 5d shows spectra acquired from various non-built up urban surfaces. The most prominent spectral features are evident in the green residential grass spectrum (1), which shows pronounced chlorophyll absorptions at 450 and 680 nm, a green peak centered at 550 nm, and vibrational water absorptions at 980, 1200, 1400 and 1900 nm. The highest reflectance was observed in landscaping bark (4), which showed prominent ligno-cellulose bands in the SWIR. Spectra of bare soil were moderately featureless, showing only a general increase in reflectance from the visible to SWIR and a subtle absorption centered at 2100 nm. Dead pine needles (5) show prominent ligno-cellulose bands with some of the lowest reflectance measured for NPV.

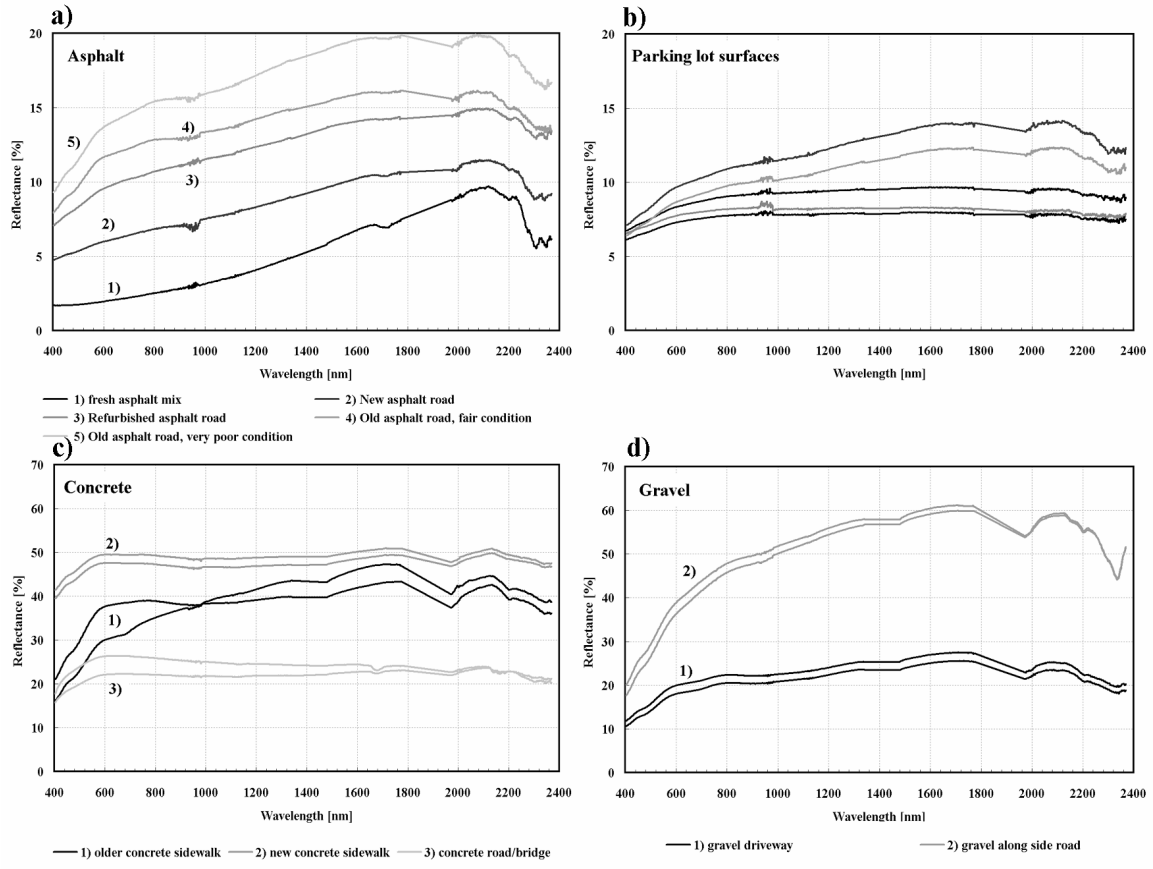

Figure 6) Spectra of typical materials of transportation surfaces from the Santa Barbara ASD urban spectral library. (a) shows asphalt spectra, (b) shows parking lots, (c) concrete sidewalks and bridges and (d) gravels.

Figure 6a-d shows spectral variations in a variety of transportation materials. Figure 6a shows the impact of aging and condition on asphalt spectra. New asphalt surfaces (1) have the lowest reflectance with increased reflectance towards 2100 nm and an overall convex shape. The most prominent absorption features occur around 2350 nm. Aging and deterioration result in a general increase in asphalt reflectance in all parts of the spectrum. The natural aging of asphalt is caused by reaction with atmospheric oxygen, photochemical reactions with solar radiation, and the influence of heat, resulting in the loss of oily components by volatility or absorption, changes of composition by oxidation, and changes in molecular structuring (Bell, 1989). Short-term losses of oily compounds produce dramatic differences between new and fresh asphalt (2). In a relatively short period of time, newly lain asphalt nearly doubles in reflectance with reduced expression of the 2350 nm absorption. Long-term aging due to oxidation and photochemical reactions produces increasing reflectance in older, more damaged surfaces due to continued loss of oily components and the loss of the sealing tar surface and the accumulation of dirt and dust. The oxidation process is clearly shown by the appearance of iron-oxide absorption features at 520 nm, 670 nm and 870 nm, especially in spectra 4 and 5. In general, the distinct spectral variations that represent the aging and condition of asphalt surfaces represent an interesting spectral contrast that might be used to map road age and specific conditions using imaging spectrometry. The most featureless, low reflectance spectra were located in parking lots (Fig. 6b). Reflectance in parking lots varied from an average around 8% to a high around 13%. Spectral features are completely absent in many of the spectra.

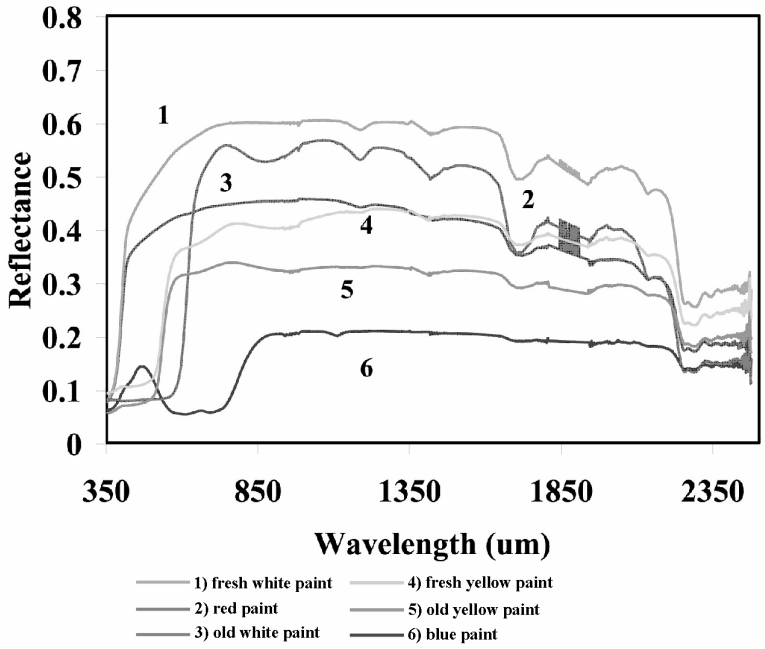

Figure 7) Spectra of typical paints from the Santa Barbara ASD urban spectral library.

Spectra of dry concretes are shown in Figure 6c. The highest reflectance was observed in fresh concrete, which showed only subtle absorptions in the SWIR. Material aging and degraded conditions resulted in an overall decrease in reflectance. Decreasing surface reflectance most likely reflects the impact of dust and dirt accumulating on the surface. Older concrete surfaces (1) also show subtle absorptions potentially due to iron-oxides and clay and carbonate absorptions in the SWIR. Low reflectance on the concrete bridge was largely due to darkening by skid marks and rubber left by tires. Figure 6d shows spectra of two gravel surfaces, gravel along the side of a road (2) and a gravel drive way (1). Prominent vibrational bands are

evident in the SWIR in road gravel, most likely due to the presence of calcium carbonate within the rock mix.

Some of the most distinctive spectra have no natural analogs (Fig. 7). This figure shows the spectra of paints commonly used on road surfaces, parking lots and curbs in the USA. Spectra include fresh white paint (1), old white paint (3), red paint (2), fresh and old yellow paint (4 and 5) and blue paint (6). A common feature to all paint spectra is a broad absorption covering several hundred nm in the SWIR. As in concretes, older paints typically show a decrease in reflectance. Blue paint shows a striking similarity to a mixture between asphalt and trees, suggesting some potential for confusion.

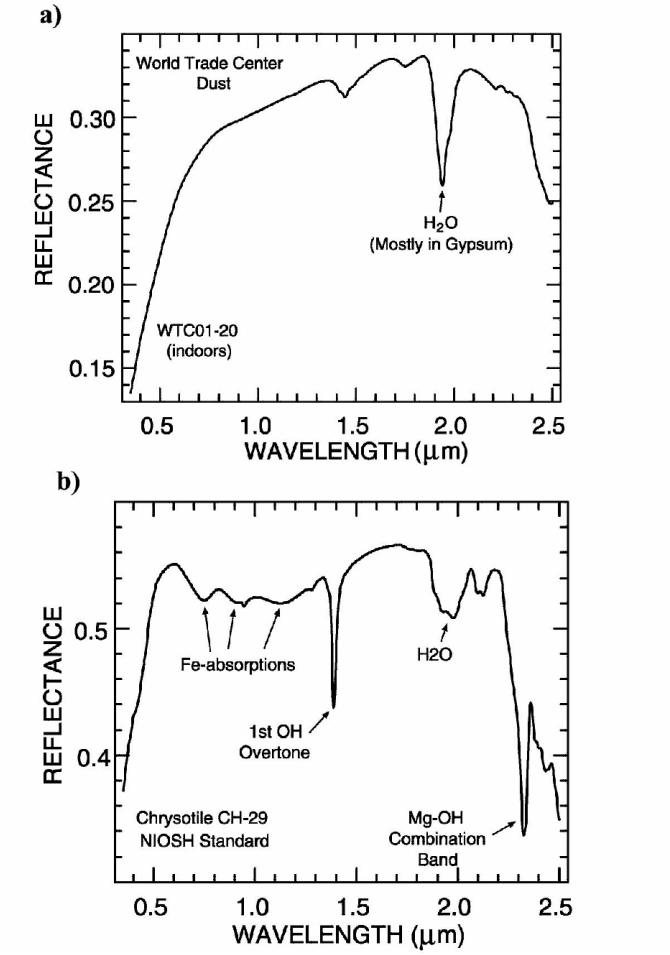

Figure 8) a) Spectra of dust collected from the vicinity of the World Trade Center and b) of chrysotile asbestos. Modified from original figures published in Clark *et al.* (2001).

Figure 8 shows an example of gypsum and the asbestiform mineral chrysotile (from Clark *et al.* 2001). These spectra were collected as part of rapid emergency response after the World Trade Center disaster in an effort to map potential environmental contaminants (Clark *et al.* 2001). Figure 8a shows several prominent vibrational bands, including a strong liquid water band centered at 1.94 ? m, a weaker water/OH absorption at 1.45 ? m and a triplet of diagnostic absorptions for gypsum between 1.42 and 1.54 ? m, probably derived from crushed wall board (Clark *et al.* 2001). Clark *et al.* (2001) also cite subtle evidence for portlandite or muscovite, minerals commonly found in concretes. Figure 8b shows the spectrum of chrysotile, an asbestiform mineral with prominent iron absorptions in the VNIR, and prominent vibrational

bands in the SWIR. A key objective of the analysis of AVIRIS images acquired over the World Trade Center in September, 2001, was to determine whether abestiform dust was present at harmful levels based on the presence of chysotile- specific absorption features in image data (see below).

QUANTIFICATION AND/OR SPECTRAL MANIPULATION AND/OR DATA PROCESSING

Data preprocessing

As stated previously, spectra are most readily interpreted when they are transformed into reflectance. The process of converting measured radiance or DNs to reflectance has been called reflectance retrieval. Techniques for retrieving surface reflectance can be roughly divided into two major categories, relative reflectance retrieval techniques and absolute reflectance retrieval techniques. The most common approach for relative reflectance retrieval is called the empirical line (Roberts *et al*. 1985). Using this approach, two or more targets of known reflectance are located in an image. A linear equation is established for each wavelength by regressing known reflectance against measured radiance or DNs. The advantage of an empirical line calibration is that radiometric calibration (conversion of DNs to radiance) is not a requirement. However, it does make the assumption that the atmosphere is uniform, resulting in significant artifacts in strong atmospheric bands (e.g., water vapor, CO_2) if a range of elevations are present in the scene (Roberts *et al*. 1993).

Absolute approaches retrieve surface reflectance based on physical principles, in which measured radiance is typically compared to radiance generated by an atmospheric radiative transfer model, such as the Moderate Spectral Resolution Atmospheric Transmittance Algorithm and Computer Model (MODTRAN: Berk *et al*. 1999). This general approach is commonly referred to as forward-inversion. Accurate radiometric calibration of the data is a fundamental requirement of forward-inversion. One of the greatest sources of error in forward-inversion is spectral calibration. For example Green (1998), documents relatively large errors in reflectance retrieval, associated with spectral calibration errors of a few nm or less. A number of authors have developed models that have the capability of retrieving surface reflectance from imaging spectrometry data. For example, Green *et al*. (1993) describe a model in which the program MODTRAN is used to build a look up table of radiance modeled with different amounts of atmospheric water vapor. Residuals between measured and modeled radiance are calculated and the best model is selected that minimizes the residual within the spectral fit region. This model also includes variables that account for the expression of liquid water in spectra, generating maps of water vapor, liquid and surface reflectance. Similar models have also been developed by Gao *et al*. (Atmospheric Removal (ATREM): 1993; 1997) and are commercially available such as ACORN (Atmospheric Correction Now, IMspec Associates). Surface reflectance retrieved through forward-inversion often shows minor artifacts along the flanks of strong water vapor bands and can show systematic errors in reflectance. To minimize these artifacts, a single reflectance spectrum of a ground target can often be used to compensate for differences between measured and modeled radiance (Clark *et al*. 2002). Figure 9 shows an example of such an approach, in which reflectance measured from one ground target in Canada, was used to adjust retrieved reflectance for a large number of AVIRIS scenes acquired during the Boreas mission in central Saskatchewan and northern Manitoba in 1994 (Roberts *et al*. 1999). High frequency artifacts can also be suppressed in the absence of ground data using spectral polishing approaches such as EFFORT (Boardman, 1998). Errors in retrieved water vapor, can seriously impact surface reflectance by generating artifacts along the margins of water vapor bands as shown by Green (2001).

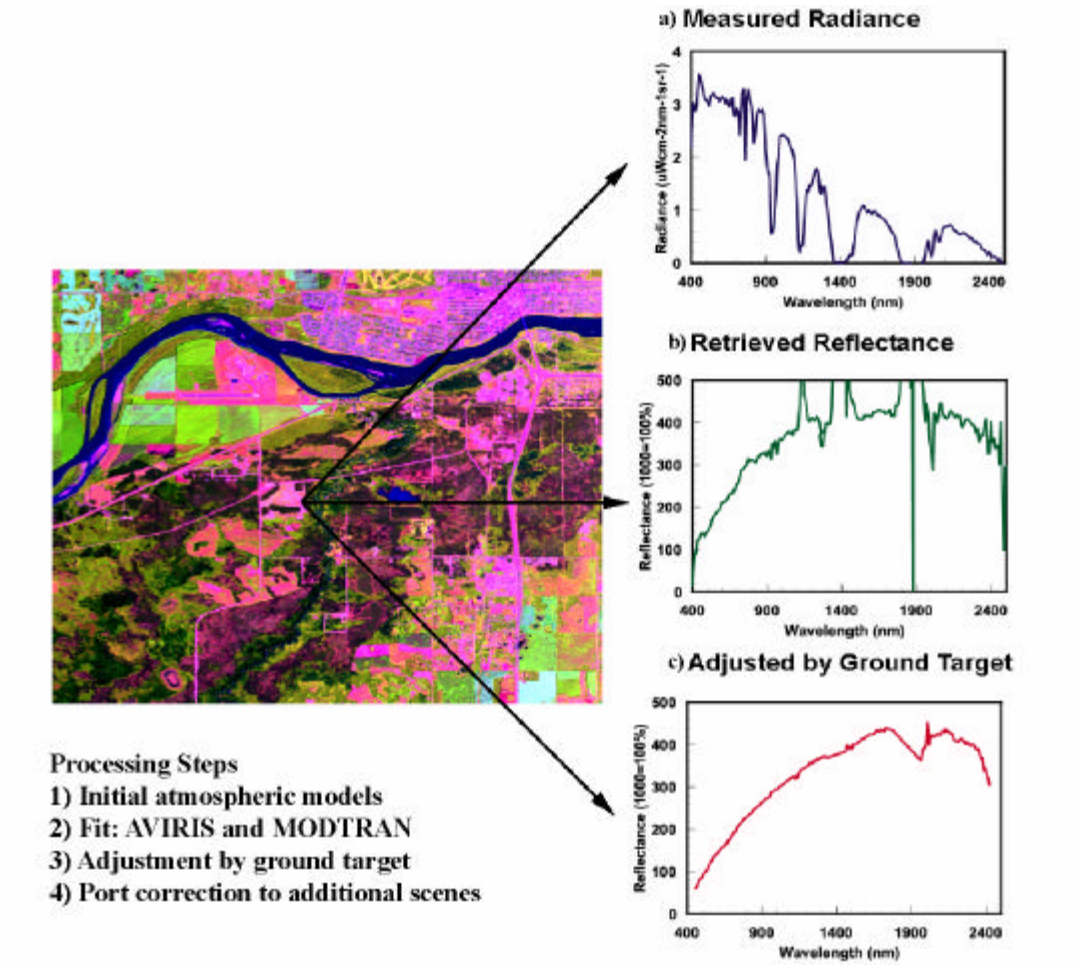

Figure 9) Schematic figure showing the process of retrieving surface reflectance from AVIRIS data. The image to the left was acquired during the 1994 Boreas campaign. (a) shows a radiance spectrum measured by AVIRIS from a field calibration target. (b) shows the first iteration of reflectance retrieved using the approach described by Green et al. (1993). (c) shows surface reflectance calculated using a field spectrum to correct for artifacts.

Reflectance retrieval in urban areas can be further complicated by atmospheric pollutants, which typically do not have a uniform distribution in space and can vary throughout the day. Atmospheric pollutants most typically impact scattering at shorter wavelengths. In most absolute reflectance retrieval approaches, they are accounted for by varying the atmospheric visibility, but not allowed to vary spatially. Thus spatially varying scattering due to atmospheric pollutants is typically not corrected.

Another common preprocessing step is georectification. Unlike spaceborne data, aircraft data are subject to considerable distortion due to the instability of low altitude platforms. In order to make maps and relate them to ground reference data, it is critical that aircraft-related and ground-related distortions are removed. One common approach is to use a "rubber-sheet" stretching approach and numerous tie points between a base map and measured image (Wiemker *et al.*, 1996). Unfortunately, this approach is not practical for highly unstable platforms, such as the Twin-Otter, which is used to acquire high spatial resolution AVIRIS. Fortunately, recent improvements in on-board navigation information and recent software development

have made it possible to georectify images to within a few pixels (~10 m for a 4 m GIFOV) in a near-automated fashion (Boardman, 1999).

Several techniques have also been developed for spectral preprocessing. One of the most common approaches for data reduction is the Minimum Noise Fraction (MNF) transform (Green *et al*. 1988). The MNF transform is similar to a Principal Components Analysis, in which a population of spectra is transformed by a set of orthogonal vectors that account for progressively less of the spectral variability. The first few MNF bands typically account for a majority of the variance, and higher MNF bands are dominated by sensor noise. As spectral dimensionality increases, the number of MNF bands required to account for signal increases, approaching over 30 dimensions in some cases. Many spectral analysis techniques (see below) are applied to data after they have been reduced by an MNF transform.

Another common spectral preprocessing technique is called continuum removal (Clark and Roush, 1984). The continuum can be defined as a spectrum that lacks all major high frequency absorptions. Mustard and Sunshine (1999) define it as "the collective properties of spectral regions exhibiting smoothly varying spectral properties that, taken as a whole, define the upward limit of the general reflectance curve for a material". Continua, which vary from one spectrum to the next, are typically fit by connecting regions of peak reflectance, and bridging absorption features with a tangent line. Continuum removal involves calculating the ratio of the measured spectrum, divided by the spectrum of its continuum. Continuum removal is useful in that it accentuates more subtle absorption features, and normalizes brightness differences. However, it may also be problematic if the spectral response of the mineral is weak and depends on the wavelength bounds used to define the continuum.

Spectral matching techniques

A large number of tools have been developed for matching a library of known spectra to spectra measured in the field or by an imaging spectrometer. Currently, the most common approach for spectral matching in urban remote sensing is the use of standard supervised classification techniques, in which spectra are acquired from a number of known targets (known as training sites) and used to determine the statistical properties of each class (Richards, 1993). Examples in which a maximum likelihood classifier (MLC) was applied to urban imaging spectrometry to map urban land cover include McKeown *et al.* (1999), Roessner *et al.* (2001) and Herold *et al.* (2003). Once training sites have been established, training statistics are extracted (typically a mean and variance) for each class, then the classifier is used to assign a pixel to one of several classes based on its statistical similarity to a particular class.

Other approaches more explicitly designed for the analysis of imaging spectrometry data have also been designed. Examples include the Spectral Angle Mapper (SAM; Kruse *et al*. 1993), in which the angle between a reference spectrum and an unknown is calculated as the inverse cosine of the product of the transpose of one vector, multiplied by the other, divided by the product of the lengths of the two vectors:

$$\theta = \cos^{-1}[a^{T}b/(||a||*||b||)]$$

where θ is the angle between two vectors, a and b, and $||a||$ and $||b||$ are each vector lengths. The key to this approach is that any spectrum can be treated as a vector in n-dimensional space emanating from the origin. To map a material, a spectrum is selected as a reference, then the angle between this reference and a spectrum in the image is calculated. To map multiple materials, multiple references are selected and unknowns are assigned to the reference that produces the smallest angle. Spectral angles that exceed a pre-

defined threshold (say 2 degrees) for all reference spectra are commonly masked out. McKeown *et al.* (1999) used SAM in addition to a MLC in their analysis.

A number of techniques have been developed in which spectra are modeled as linear combinations of vectors. One of the most common approaches is Spectral Mixture Analysis (SMA), in which a mixed spectrum is modeled as the sum of "pure" spectra, each weighted by the fraction of the material within the field of view. SMA is a powerful approach, in that it provides estimates of surface abundance as well as composition. However simple SMA, in which one set of endmembers is used to "unmix" an entire scene is poorly suited for urban areas due to the large number materials within the scene. To compensate for these limitations Roberts *et al.* (1998) have developed Multiple Endmember Spectral Mixture Analysis (MESMA), in which the number and types of endmembers are allowed to vary per pixel. Although MESMA has been primarily applied to natural systems, early applications in urban areas seem promising (Gardner *et al.* 2001). An alternate approach was used by Roessner *et al.* (2001) to account for considerable spectral variability in an urban area. Roessner *et al.* (2001) used a MLC to first identify relatively unmixed spectra, which could then be used as candidate endmembers. Once identified, these spectra were used as seeds to unmix neighboring pixels and calculated mixtures.

Several alternative linear transformations have been proposed for the analysis of imaging spectrometer data. Harsanyi and Chang (1994) first introduced the concept of orthogonal subspace projection, in which spectra are transformed into a set of orthogonal vectors. Vectors are calculated such that spectral features that are not of interest produce a low score, and spectra that match the material of interest produce a high score. Variations on orthogonal subspace projection include Matched Filters, Foreground/Background Analysis (Smith *et al.* 1994), and Mixture Tuned Matched Filters (MTMF: Boardman *et al.* 1995). Ben-Dor *et al.* (2001) and Ben-Dor (2001) use a MTMF and ten endmembers to classify CASI data acquired over Tel-AVIV, Israel. We provide an example using a Matched Filter later in the chapter.

Spectral fitting represents another powerful analysis tool. An example of this is Tetracorder (Clark *et al.* 2003), in which spectra first undergo continuum removal, then a non-linear least squares approach is used to choose the best candidate among a series of reference materials based on the highest fit. Specific minerals are typically mapped using fit regions tailored to provide the best discrimination for that type of absorption feature. For example, iron-oxides are typically mapped using a different fit region than clays. Clark *et al.* (2001) provide an example of Tetracorder, in which references samples of various dusts and asbestiform minerals are used to map candidate materials in the vicinity of the World Trade Center disaster.

EXCEPTIONAL ASPECTS OF THE TECHNIQUE

The fine scale of urban objects and the high diversity of surface materials severely complicate the use of remote sensing in these areas. Currently, spaceborne imaging spectrometers lack sufficient spatial resolution to be used for many urban applications. In contrast, airborne systems commonly meet a minimum standard of 5 m or less and provide considerably greater spectral detail than aerial photography and broad band images. Currently the major limitation on the use of imaging spectrometry is cost and the availability of data.

In many instances, the added spectral information provided by an imaging spectrometer does not provide sufficient benefits to justify its use place of more inexpensive broad band or photographic sources. However, in the instance where a specific wavelength region is required to map a material based on a particular absorption feature, the use of an imaging spectrometer is justified. Examples discussed in this chapter include:

Separation of wood shingle from other roof types

Sensors such as IKONOS and Quickbird are incapable of mapping these roof types at high accuracy. In contrast, imaging spectrometers can definitively identify these roof types based the presence of ligno-cellulose bands in the SWIR. According to Herold *et al.* (2003), a broad band system such as Landsat TM can map wood shingle, although the lack of spectral detail in the SWIR is also likely to lead to greater confusion with other materials.

Environmental contaminants

Clark *et al.* (2001) demonstrated the potential of an imaging spectrometer for mapping environmental contaminants in the aftermath of the World Trade Center disaster. In the case where diagnostic absorptions are required to map a specific mineral, an imaging spectrometer may be the only practical means.

Very little is still known about the spectra of urban materials. Considerably more research has focused on natural materials such as plants, rocks and minerals. It is possible, given more research that comprehensive libraries will be developed, increasing our ability to map specific materials based on diagnostic absorptions. In the absence of more detailed knowledge of urban spectrometry, however, imaging spectrometers have been shown to provide improved discrimination and land-cover mapping (e.g. Herold *et al.* 2003).

Fundamentally, multispectral systems are limited spectrally and must rely to a greater extent on spatial patterns to map land-cover. Using an approach such as MESMA, the potential exists for mapping hundreds of distinct materials by allowing the number and types of endmembers to vary on a per pixel basis. Whereas many materials are likely to remain problematic (i.e. asphalt roads and composite shingle), others can be readily discriminated based on their spectra.

Techniques such as MTMF (Boardman *et al*. 1995), could potentially be employed to produce detailed maps of materials below the resolution of the GIFOV. The ability to locate a material will depend to a considerable extent on the spectral contrast of the material relative to its surrounding background. In other words, it may be possible to extend our ability to map a material well below the GIFOV of the instrument given a sufficient amount of spectral leverage. Tradeoffs between spatial and spectral resolution have yet to be established for an urban landscape. Experience from mineral mapping suggests that such an approach should be fruitful, given greater knowledge of the spectra of urban materials.

NOVEL APPROACHES

Examples from AVIRIS acquired in the Santa Barbara area

As part of several projects designed to evaluate the potential of hyperspectral data for mapping transportation infrastructure and roof materials, University of California Santa Barbara (UCSB) built an urban spectral library for the Goleta/Santa Barbara area. A total of 6,500 spectra were acquired between late May and early June, 2001 using an ASD full range instrument on loan from the Jet Propulsion Laboratory (Fig. 3). Once averaged and converted to reflectance, these spectra included 499 roofs, 179 roads, 66 side walks, 56 parking lots 40 road paints, 37 vegetation, 47 types of non-photosynthetic vegetation (i.e., landscaping bark), 88 bare soil and beach spectra, 27 acquired from tennis courts and 50 more from miscellaneous surfaces.

One major research question we are addressing is the feasibility of imaging spectrometers for mapping the large spectral diversity of urban materials within a highly mixed urban environment. Because unique spectral features are present in red tile and wood shingle, these materials should be relatively easy to map

(Fig. 5a, b). However, spectral similarities between other materials, such as composite shingle and asphalt surfaces (due to similar material composition) suggest significant confusion is likely to occur (Fig.5). To quantify spectral separability of materials, we employed the Bhattacharyya distance (B-distance) as a measure of spectral separability (Jimenez and Landgrebe, 1999). The B-distance is calculated using Eq.1:

$$B = \frac{1}{8}[\mu_1 - \mu_2]^T \left[\frac{\Sigma_1 + \Sigma_2}{2}\right]^{-1} [\mu_1 - \mu_2] + \frac{1}{2} \mathrm{Ln} \frac{\left|\frac{1}{2}[\Sigma_1 + \Sigma_2]\right|}{\sqrt{|\Sigma_1||\Sigma_2|}}$$

where μ_i and $?_i$ are the mean vector and the covariance matrix of classes one and two, respectively. This separability metric was developed to measure the statistical distance between two Gaussian distributions (Kailath, 1967) and incorporates both first order and second order statistics, in which the first half of Equation 1 incorporates differences in means, and the second part incorporates covariance (Landgrebe, 2000). Because the B-distance only provides relative measures of separability, it cannot be used to establish absolute thresholds. Low B-distances imply relatively lower separability.

Table 2 shows that the lowest B-distance values occurred between specific types of roofs and roads. These spectral similarities are due to generic material properties and are responsible for lower accuracies reported by Herold *et al.* (2003). In fact, spectral confusion between individual roofs and roads is higher than for different road surface types. Concrete roads and to some extent asphalt roads have fairly high average and low minimum separation. This indicates a large within class variability and emphasizes the spectral complexity of transportation surfaces compared to other urban land cover types.

Table 2) Matrix of B-distance values for minimum and average separability between different manmade land cover types.

	1: Com_sh	2: Grav_rf	3: Tar_rf	4: Gr_tile	5: Rd_tile	6: Wd_sh	7: Asp_rd	8: Concr	9: Grav_rd	10: P_lot
1: Composite shingle		56	19	14	75	61	8	18	106	13
2: Gravel roof	**405**		36	46	109	189	51	17	88	84
3: Tar roof	**190**	**599**		30	69	127	17	20	135	26
4: Gray tile roof	**92**	**178**	**67**		34	32	35	16	61	31
5: Red tile roof	**549**	**581**	**559**	**375**		84	90	52	147	130
6: Wood shingle roof	**315**	**359**	**171**	**172**	**197**		218	31	152	249
7: Asphalt road	**244**	**693**	**119**	**99**	**1331**	**351**		28	68	7
8: Concrete road	**687**	**735**	**1325**	**423**	**1247**	**977**	**1151**		29	11
9: Gravel road	**2533**	**2514**	**1733**	**2460**	**927**	**4370**	**3047**	**1799**		117
10: Parking lot	**194**	**700**	**98**	**81**	**1499**	**436**	**194**	**897**	**3832**	
Coding of values:	**Bold**: Average separability (lower left part of matrix) Italic: Minimum separability (upper right part of matrix)									
Gray background:	Average value ≤ 150 / Minimum value ≤ 20									

The B-distance can be used to design an optimal subset of spectra for mapping discriminating urban materials. Figure 10 shows spectra of nine materials and the wavelength location of 14 bands which best discriminate them. Landsat TM bands are shown in grey, illustrating that several important wavelength regions are not sampled by the Landsat system.

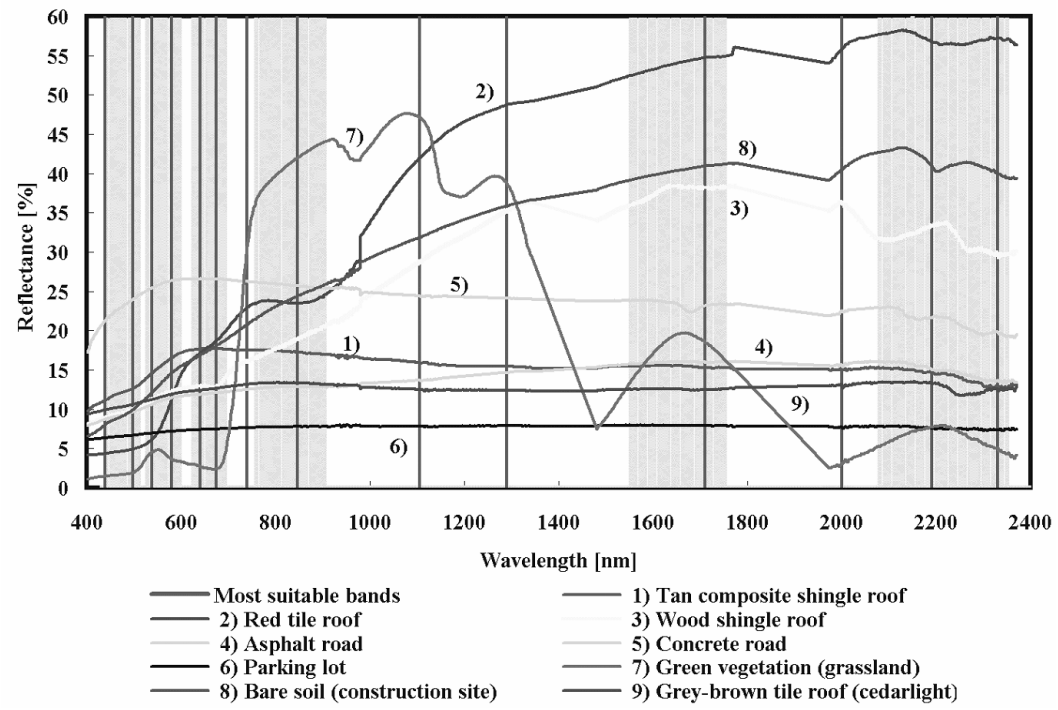

Figure 10) Most suitable spectral bands (vertical lines) for urban mapping derived from the ASD spectral library and the AVIRIS data compared to spectral signatures of several urban land cover types and the spectral coverage of LANDSAT TM satellite sensor (gray in the background).

Based on this analysis, the most suitable bands for urban mapping appear in nearly all parts of the spectrum with a fair number in the visible region (Fig. 10). This indicates that narrow spectral bands (~ 20 nm wide) are important in resolving small-scale spectral contrast (e.g. color, iron absorption features) among materials and land cover types in this spectral region. Several additional bands appear in the SWIR, some of which are associated with specific absorption features (e.g. clays) while others are responsive to large reflectance differences between materials, such as the high reflectance of red tile beyond 1000 nm.

Based on spectra of urban materials and the B-distance, we would expect some materials, such as wood shingle roofs, to be readily mapped by a sensor such as AVIRIS at very high accuracies. In contrast, we would anticipate considerable confusion between some types of roofs (mostly composite shingle) and asphalt roads. In order to test this, we employed a matched filter in the Environment for Visualizing Images (ENVI) software package to high spatial resolution AVIRIS data acquired over Goleta, California (Fig. 11). Figure 11a shows the matched filter scores for wood shingle roof; Figure 11b shows the asphalt road and Figure 11c shows a spatially georectified map of known roads and wood shingle roofs. Comparison of these three figures demonstrates that wood shingle roofs could be mapped at very high accuracies, producing high matched filter scores in virtually all areas mapped as wood shingle. The most significant false positives appear to be open fields consisting of senesced grass. In contrast, the matched filter for asphalt road shows considerable error. In Figure 11b, the matched filter correctly maps most road surfaces, but also maps large areas of dark composite shingle. One approach for reducing spectral confusion between these two material types would be to incorporate a third dimension into the analysis. For example, if LIDAR or IFSAR were used to map the height of surfaces, confusion between roads and roofs would be greatly reduced.

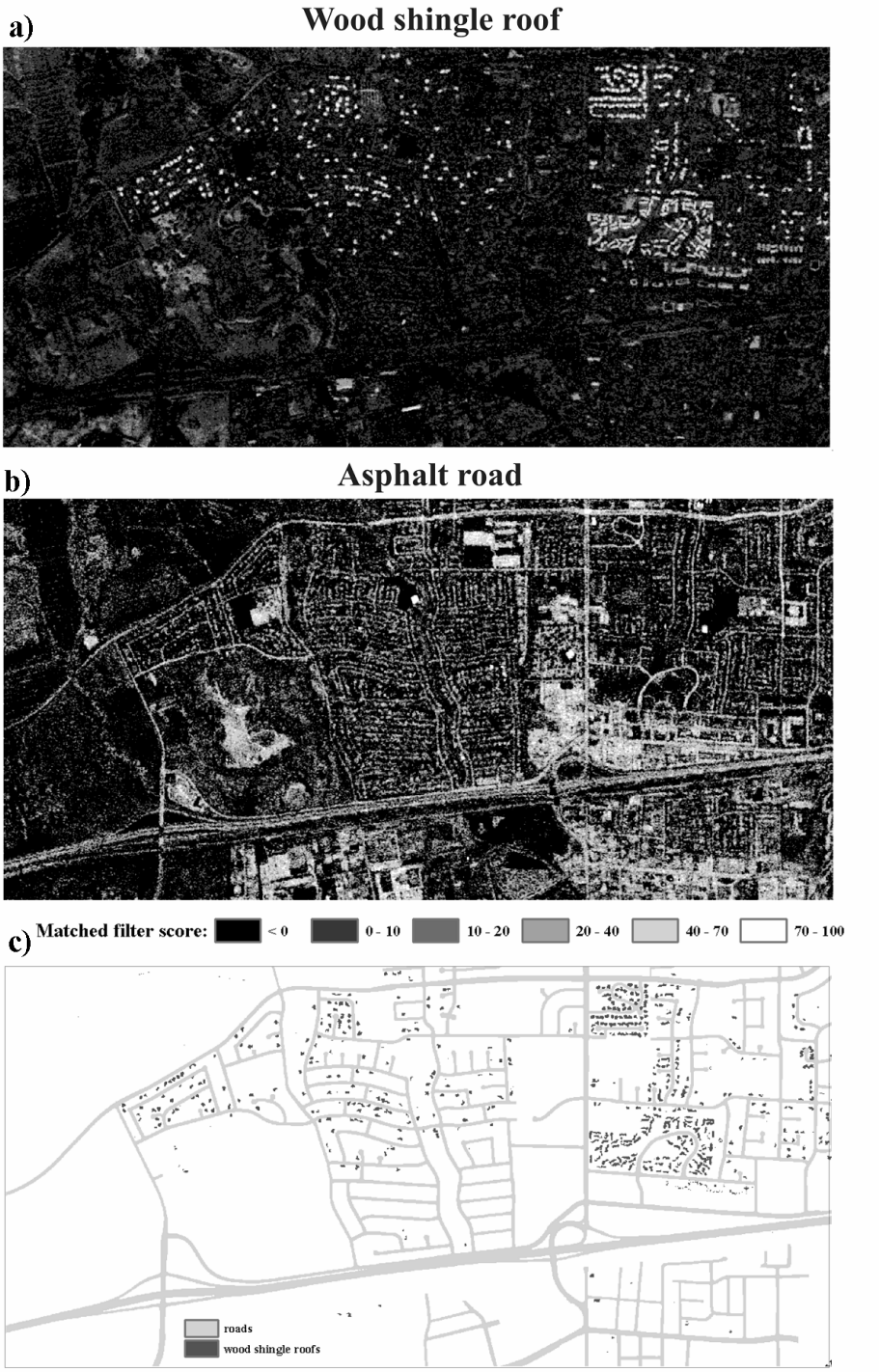

Figure 11) Results of matched filter analysis for wood shingle roofs (a) and asphalt roads (b) compared to reference data (c) for wood shingle roofs and asphalt roads.

Examples from the World Trade center

Imaging spectrometry has considerable potential to help in emergency disaster response. Potential applications of an imaging spectrometer included mapping thermal sources and environmental contaminants. Following the World Trade Center Disaster of September 11, 2001, AVIRIS was deployed

on a Twin Otter and flown to the area. A particular concern was the potential of widespread dissemination of potentially cancer causing asbestiform dusts. However, other dusts originating from crushed urban materials are also of concern due to their potential to produce respiratory problems.

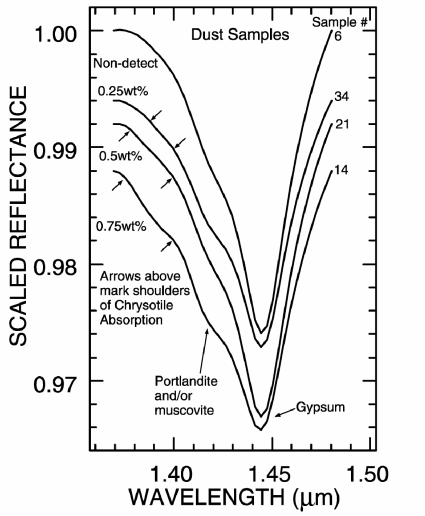

Figure 12) Spectra of World Trade Center dust with variable amounts of chrysotile asbestos. Outer edges of chrysostile absorption bands are marked by arrows. From Clark *et al.* (2001).

AVIRIS imaged the World Trade Center and its vicinity four times between September 15 and 23, 2001. Because of time constraints for emergency relief efforts, the data were radiometrically calibrated, georectified and corrected to surface reflectance as quickly as possible after image data were acquired, then analyzed using Tetracorder at the United States Geological Survey (USGS). For example, data acquired on September 16th were shipped to the USGS by September 17th and fully analyzed between September 17th and 19th using real-time feedback from field crews. Examples shown here are derived from an Open File Report published by the USGS (Clark *et al.* 2001). The reader is encouraged to read the full report.

Figure 13) Serpentine and amphibole mineral map in the vicinity of the World Trade Center, generated by Clark *et al.* (2001) using Tetracorder. A lack of color is indicative of low concentration of chrysotile or amphibole asbestos.

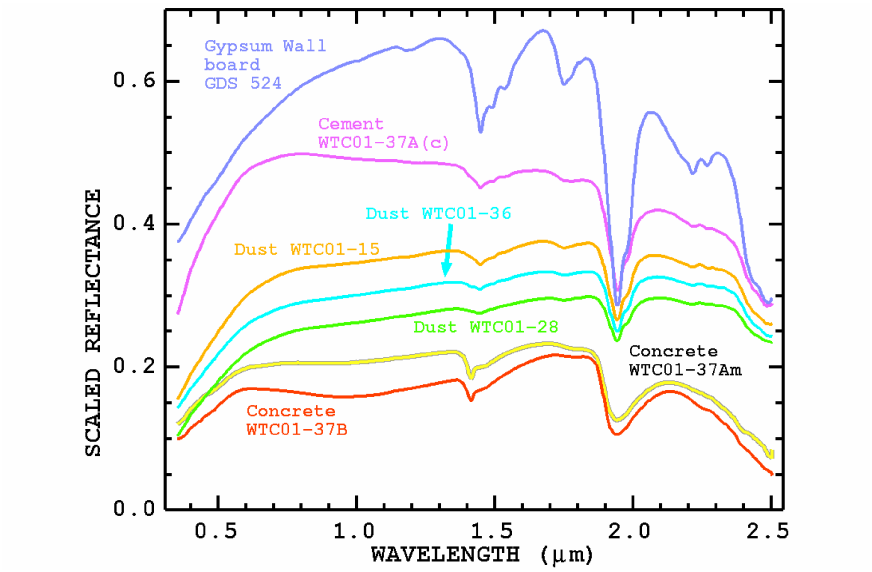

Figure 14) Spectra of various dusts and building materials. From Clark *et al*. (2001).

Researchers from the USGS collected spectra from 33 dust samples acquired in the vicinity of the two towers between September 17 and 19th, 2001. Figure 12 shows a spectral subset of several dusts determined to have variable amounts of chrysotile asbestos. Tetracorder was applied to high spatial resolution AVIRIS data to determine the extent of asbestiform dust contamination (Fig. 13). The lack of color in this figure suggests that contamination levels remained low, although there is some evident of east-west spread of chrysotile dust (Clark *et al*. 2001).

Figure 15) Dust/debris plume map in the vicinity of the World Trade Center, generated by Clark *et al.* (2001) using Tetracorder.

Crushed building materials represent a potentially large source of exotic dust. Figure 14 shows a selection of spectra, published by Clark *et al.* (2001) showing cements, gypsum wall board, concretes and dusts collected from the World Trade Center. These spectra were used as reference spectra for Tetracorder and used to map different dust types disseminated throughout the areas (Fig. 15).

Maps such as these have considerable potential in aiding relief efforts. The extremely rapidity that these data were acquired, processed and analyzed to make maps offers a glimpse of some of the potential of imaging spectrometry for rapid urban disaster response.

SUMMARY

Urban areas represent the hub of human activities, where most human commerce and population is concentrated. Remote sensing is currently undergoing a renaissance in these areas, in large part due to the availability of sensors that provide unprecedented spatial and spectral detail. Urban areas are particularly challenging for remote sensing because of the requirement of fine spatial resolution (~5 m), the high diversity of materials, complex lighting geometries (and bidirectional reflectance properties of many surfaces) and potentially variable atmospheric properties due to airborne pollutants. Airborne imaging spectrometers, by sampling a large number of wavelengths at fine spatial resolution are uniquely qualified to map urban materials at high accuracies.

In this chapter we provide a brief overview of some important aspects of urban imaging spectrometry. We provide a brief introduction documenting some recent applications of imaging spectrometry in urban areas. We follow with a discussion of important radiometric and spectral concepts, with a focus on how they apply to urban areas. We discuss instrumentation, with a focus on field instruments and sampling procedures. We also discuss airborne platforms, focusing primarily on sensors that have recently been used to map urban land cover. Airborne sensors are particularly important because they offer the potential of developing a comprehensive spectral library at relatively low cost at an appropriate spatial resolution. We illustrate important aspects of urban spectra using field spectra measured in the Santa Barbara area. We include spectra of roofs of varying materials and conditions, transportation surfaces (roads, sidewalks) and street paints. Next, we discuss analysis techniques, starting with preprocessing (including reflectance retrieval and georectification), followed by a subset methods used to identify materials. Although a large diversity of analysis techniques exist, we present only those that have been recently applied to imaging spectrometry of urban areas. We conclude the chapter with several examples of applications, including the development of a spectral library for the Santa Barbara area and the use of imaging spectrometry to map environmental contaminants at the World Trade Center. Imaging spectrometry is a rapidly evolving field in which new sensors and new analysis methods are continually being developed. Urban remote sensing represents a relatively new, but exciting application for this technology. The combination of technologies, such as LIDAR, which can provide a vertical description of a landscape, and imaging spectrometry, which provides improved spectral discrimination, is particularly powerful.

ACKNOWLEDGEMENT

The ASD field spectrometer was kindly supplied by the NASA Jet Propulsion Laboratory. The author acknowledges the support of the U.S. Department of Transportation, Research and Special Programs Administration, OTA #DTRS-00-T-0002 (NCRST-Infrastructure), NASA EO1-Science Validation (NCC5-496), Solid Earth and Natural Hazards (NAG2-1140) and regional Earth Science Application Center (RESAC) programs (CSDH NASA RESAC 447633-59075).

REFERENCE LIST

ANDERSON, J.R., HARDY, E.E., ROACH, J.T., & WITMER, R.E. (1976): A Land Use and Land Cover Classification Scheme for Use with Remote Sensor Data, U.S. Geological Survey Professional Paper 964.

BELL, C.A. (1989): Summary Report on the Aging of Asphalt-Aggregate Systems, Strategic Highway Research Program (SHRP) Publications SHRP-A-305, 100 p., URL: http://gulliver.trb.org/publications/shrp/SHRP-A-305.pdf (access: September 2002).

BEN-DOR, E. (2001): Imaging Spectrometry for Urban Applications, in *Imaging Spectrometry*, (Van der Meer, F.D., and de Jong, S.M. (Eds), Kluwer Academic Publishers, Netherlands, 243-281.

BEN-DOR, E., LEVIN N., & SAARONI, H. (2001): A spectral-based recognition of the urban environment using the visible and near-infrared spectral region (0.4-1.1 m). A case study over Tel-Aviv, *Int. J. Remote Sens.*, 22 (11), 2193-2218.

BERK, A., ANDERSON, G.P., BERNSTEIN, L.S., ACHARYA, P.K., DOTHE, H., MATTHEW, M.W., ADLER-GOLDEN, S.M., CHETWYND, J.H. Jr., RICHTSMEIER, S.C., PUKALL, B., ALLRED, C.L., JEONG, L.S., & HOKE, M.L. (1999): MODTRAN4 Radiative Transfer Modeling for Atmospheric Correction, *in* Proceedings of SPIE Optical Spectroscopic Techniques and Instrumentation for Atmospheric and Space Research III, 19-21 July, 1999, Vol. 3756, 6 pp.

BIANCHI, R., CAVALLI, R.M., FIUMI, L., MARINO, C.M., PANUZI, S. & PIGNATTI, S. (1996): Airborne Remote Sensing in Urban Areas: Examples and Considerations on the Applicability of Hyperspectral Surveys over Industrial, Residential and Historical Environments, *in* the Second International Airborne Remote Sensing Conference and Exhibition I: San Francisco, CA, 439-444,

BOARDMAN, J.W. (1998), Post-ATREM polishing of AVIRIS apparent reflectance data using EFFORT: a lesson in accuracy versus precision, *in* Summaries of the 8th JPL Airborne Earth Science Workshop ed) Green, R.O., *JPL Publication 99-17*, Pasadena, CA 1 p.

BOARDMAN, J.W. (1999): Precision geocoding of low altititude AVIRIS data: Lessons learned in 1998, *in* Summaries of the 8th JPL Airborne Earth Science Workshop (ed.) Green, R.O., *JPL Publication 99-17*, Pasadena, CA 63-68.

BOARDMAN, J.W., KRUSE, F.A., & GREEN, R.O. (1995): Mapping target signatures via partial unmixing of AVIRIS data *in* Summaries of the 5th JPL Airborne Earth Science Workshop (ed.) Green, R.O., *JPL Publication 95-1*, Vol 1, Pasadena, CA, 23-26.

CLARK, R.N. (1999): Spectroscopy of Rocks and Minerals and Principles of Spectroscopy, in *Remote Sensing for the Earth Sciences, Manual of Remote Sensing 3rd Ed*. Vol. 3 (ed.) Rencz, A.N., John Wiley & Sons, Inc. NY, 3-52.

CLARK, R.N., GREEN, R.O., SWAYZE, G.A., MEEKER, G., SUTLEY, S., HOEFEN, T.M., LIVO, K.E., PLUMLEE, G., PAVRI, B., SARTURE, C., WILSON, S., HAGEMAN, P., LAMOTHE, P., VANCE, J.S., BOARDMAN, J., BROWNFIELD, I., GENT, C., MORATH, L.C., TAGGART, J., THEODORAKOS, P.M., & ADAMS, M. (2001): Environmental Studies of the World Trade Center area after the September 11, 2001 attack, *U.S. Geological Survey, Open File Report OFR-01-0429* (http://pubs.usgs.gov/of/2001/ofr-01-0429).

CLARK, R.N. & ROUSH, T.L. (1984): Reflectance spectroscopy: quantitative analysis techniques for remote sensing applications, *J. Geophys. Res.* 89, 6329-6340

CLARK, R.N., SWAYZE, G.A., LIVO, K.E., KOKALY, R.F., KING, T.V.V., DALTON, J.B., VANCE, S., ROCKWELL, B.W., HOEFEN, T., and MCDOUGAL, R.R. (2002): Surface reflectance calibration of terrestrial imaging spectroscopy data, in Proceedings of the Eleventh JPL Airborne Earth Science Workshop , (ed.) Green R.O., *JPL Publication 03-04*. 43-64. (http://speclab.cr.usgs.gov/PAPERS.calibration.tutorial/).

CLARK, R.N., SWAYZE, G.A., LIVO, K.E., KOKALY, R.F., SUTLEY, S.J., DALTON, J.B., MCDOUGAL, R.R., & GENT, C.A. (2003): Imaging spectroscopy: Earth and planetary remote sensing with the USGS Tetracorder and expert systems, *J. Geophys. Res.*, 108(E12), 5131, doi:10.1029/2002JE001847, December, 2003. http://speclab.cr.usgs.gov/PAPERS/tetracorder

GAMBA, P. & HOUSHMAN, B. (2001): Integration of Hyperspectral and IFSAR data for Improved 3D Urban Profile Reconstruction, *Photogram. Eng. Remote Sens.* 67 (8), 947-956.

GAO, B.C. HEIDEBRECHT, K.B. & GOETZ, A.F.H. (1993): Derivation of Scaled Surface Reflectances from AVIRIS Data, *Remote Sens. Environ.*, 44, 165-178.

GAO, B.C., HEIDEBRECHT, K.B. & GOETZ, A.F.H. 1997): *Atmosphere Removal Program ATREM) Version 3.0 User's Guide*, Center for the Study of Earth from Space, University of Colorado, Boulder, pp 1-27.

GARDNER, M.E., ROBERTS, D.A., FUNK, C. & NORONHA, V. (2001): Road extraction from AVIRIS using spectral mixture and Q-tree filter techniques, *in* Proceedings of the tenth AVIRIS Earth Science Workshop, (ed.) Green, R.O., *JPL Publication* 02-1. Pasadena, CA, 145-150

GREEN, A.A., BERMAN, M., SWITZER, B. & CRAIG, M.D. (1988): A transformation for ordering multispectral data in terms of image quality with implications for noise removal, *IEEE Trans Geoscience Remote Sens*., 26(1), 65-74.

GREEN, R.O., CONEL, J.E. & ROBERTS, D.A. (1993): Estimation of Aerosol Optical Depth, Pressure Elevation, Water Vapor and Calculation of Apparent Surface Reflectance from Radiance Measured by the Airborne Visible-Infrared Imaging Spectrometer (AVIRIS) Using MODTRAN2, *SPIE Conf. 1937, Imaging Spectrometry of the Terrestrial Environment* (ed.) Vane, G., The Society of Photo-Optical Instrumentation Engineers, Orlando FL, 2-5.

GREEN, R.O. (2001): Atmospheric water vapor sensitivity and compensation requirement for Earth-looking imaging spectrometers in the solar-reflected spectrum *J. Geophys. Res. Atm.*, 106(D15), 17443-17452.

GREEN, R.O. (1998): Spectral Calibration Requirement For Earth-Looking Imaging Spectrometers in the Solar-Reflected Spectrum. *Applied Optics*, 37(4), 683-690.

GREEN, R.O., EASTWOOD, M.L., SARTURE, C.M., CHRIEN, T.G. ARONSSON, M., CHIPPENDALE, B.J., FAUST, J.A., PAVRI, B.E., CHOVIT, C.J., SOLIS, M.S., OLAH, M.R. & WILLIAMS, O. (1998): Imaging spectroscopy and the Airborne Visible Infrared Imaging Spectrometer, *Remote Sens. Environ.*, 65(3), 227-248.

GREEN, R.O. & PAVRI, B. (2002): AVIRIS Inflight Calibration Experiment Results for 2001, *in* Proceedings of the 2002 AVIRIS Earth Science Workshop, (ed.) Green, R.O., *JPL Publication* 03-4, Pasadena, CA, 125-138.

HARSANYI, J.C. & CHANG, C.I. (1994): Hyperspectral image classification and dimensionality reduction: an orthogonal subspace projection approach. *IEEE Trans Geosci. Remote Sens.*, 32(4): 779-785.

HEIDEN, U., ROESSNER, S., SEGL, K. & KAUFMANN, H. (2001): Analysis of spectral signatures of urban surfaces for their area-wide identification using hyperspectral HyMap data *in* Proceedings of IEEE/ISPRS Joint Workshop on Remote Sensing and Data Fusion in Urban Areas, Rome, 173-177.

HEPNER, G.F., HOUSHMAND, B., KULIKOV, I. & BRYANT, N. (1998): Investigation of the integration of AVIRIS and IFSAR for urban analysis, *Photogramm. Eng. Remote Sens*., 64 (8*)*, 813 – 820.

HEROLD, M., GARDNER, M., & ROBERTS, D. (2003): Spectral resolution requirements for mapping urban areas, *IEEE Trans. Geosci. Remote Sens.*, 41(9), 1907-1919.

JENSEN, J.R., & COWEN, D.C. (1999): Remote sensing of urban/suburban infrastructure and socio-economic attributes, *Photogramm. Eng. Remote Sens.*, 65 (5), 611-622.

JIMENEZ, L. & LANDGREBE, D.A. (1999): Hyperspectral data analysis and supervised feature reduction via projection pursuit, *IEEE Trans. Geosci. Remote Sens*., 37 (6*)*, 2653-2667,

KAILATH, T. (1967): The Divergence and Bhattacharyya Distance Measures in Signal Selection. *IEEE Trans*. *Communication Theory*, 15, 152-160.

KRUSE, F. (1999): Visible and Infrared: Sensors and Case Studies, in *Remote Sensing for the Earth Sciences, Manual of Remote Sensing 3rd Ed. Vol. 3* (ed) Rencz, A.N., John Wiley & Sons, NY, 567-612.

KRUSE, F.A., LEFKOFF, A.B., BOARDMAN, J.B., HEIDEBRECHT, K.G., SHAPIRO, A.T., BARLOON, P.J. & GOETZ, A.F.H. (1993): The Spectral Image Processing System (SIPS)- Iterative Visualization and Analysis of Imaging Spectrometer Data, *Remote Sens. Environ*., 44, 145-163.

LANDGREBE, D.A. (2000): Information Extraction Principles and Methods for Multispectral and Hyperspectral Image Data, *in* Information Processing for Remote Sensing, Chapter 1, (ed). Chen, C.H. World Scientific Publishing Co., URL: http://dynamo.ecn.purdue.edu/ ~landgreb/publications.html (access September 2002)

MCKEOWN, D.M. Jr., COCHRAN, S.D., FORED, S.J., MCGLONE, J.C., SHUFELT, J.A. & YOKUM, D.A. (1999): Fusion of HYDICE Hyperspectral Data with Panchromatic Imagery for Cartographic Feature Extraction, *IEEE Trans. Geosci. Remote Sens.*, 37(3), 1261-1277.

MCNEILL, J.R. (2000): *Something new under the sun, An environmental history of the twentiety-century world*, W.W. Norton and Company, NY, 421 pp.

MEDINA, M.A. (2000): Effects of shingle absorptivity, radiant barrier emissivity, attic ventilation flowrate, and roof slope on the performance of radiant barriers, *Int. J. Energy Res.*, 24(8), 665-678.

MUSTARD, J.F. & SUNSHINE, J.M. (1999): Spectral Analysis for Earth Science: Investigations Using Remote Sensing Data, in *Remote Sensing for the Earth Sciences, Manual of Remote Sensing 3rd Ed. Vol. 3* (ed) Rencz, A.N., John Wiley & Sons, NY, 251-306.

PRICE, J.C. (1995): Examples of high resolution visible to near-infrared reflectance and a standardize collection for remote sensing studies, *Int. J. Remote Sens.* 16, 993-1000.

RICHARDS, J.A. (1993), *Remote Sensing Digital Image Analysis, An Introduction*, Springer-Verlag, New York, 340 pp.

RIDD, M.K. (1995): Exploring a V-I-S- (vegetation – impervious surface- soil) model for urban ecosystem analysis through remote sensing: comparative anatomy for cities, *Int. J. Remote Sens. 16*, 2165-2185.

ROBERTS, D.A., ADAMS, J.B., & SMITH, M.O. (1993): Discriminating Green Vegetation, Non-Photosynthetic Vegetation and Soils in AVIRIS Data, *Rem. Sens. Environ.*, 44 (2/3), 255-270.

ROBERTS, D.A., GARDNER, M., CHURCH, R., USTIN, S., SCHEER, G. & GREEN, R.O., (1998): Mapping Chaparral in the Santa Monica Mountains using Multiple Endmember Spectral Mixture Models, *Rem. Sens. Environ.* 65, 267-279.

ROBERTS, D.A., USTIN, S.L., OGUNJEMIYO, S., GREENBERG, J., DOBROWSKI, S.Z., CHEN, J. & HINCKLEY, T.M. (2003): Spectral and Structural Measures of Northwest Vegetation at Leaf to Landscape Scales, *Ecosystems*, in press.

ROBERTS, D.A., YAMAGUCHI, Y., & LYON, R.J.P. (1985): =alibration of Airborne Imaging Spectrometer Data to Percent Reflectance using Field Spectral Measurements, *in* Proceedings of the 19th International Symposium on Remote Sensing of Environment, Ann Arbor, Michigan, October 21-25, 1985, 679-688.

ROESSNER, S., SEGL, K. HEIDEN, U. & KAUFMANN, H. (2001): Automated differentiation of urban surfaces based on airborne hyperspectral imagery, *IEEE Trans. Geosci. Remote Sens. 39 (7):* 1525 – 1532.

SABOL, D.E., ADAMS, J.B., & SMITH, M.O. (1992): Quantitative sub-pixel spectral detection of targets in multispectral images, *J. Geophys. Res.* 97, 2659-2672.

SCHOTT, J.R. (1997): *Remote Sensing, the Image Chain Approach*, Oxford University Press, NY, 394 pp.

SCHUELER, T.R. (1994): The importance of imperviousness. *Watershed Protection Techniques*, 1, 3, 100–111.

SMITH, M., ROBERTS, D., HILL, J., MEHL, W., HOSGOOD, B., VERDEBOUT, J., SCHMUCK, G., KOECHLER, C. & ADAMS, J. (1994): A new approach to quantifying abundances of materials in multispectral images, *in* Proceedings of IGARRS'94, Pasadena, CA, Aug 8-12, 2372-2374.

SWAYZE, G.A., CLARK, R.N., GOETZ, A.F.H., CHRIEN, T.G., and GORELICK, N.S. (2003): Effects of spectrometer band pass, sampling, and signal-to-noise ratio on spectral identification using the Tetracorder algorithm, *J. Geophys. Res*., 108(E9), 5105, doi: 1029/2002JE001975, 30 p.

UNGAR, S. PEARLMAN, J. MENDENHALL, J. & REUTER, D. (2003): Overview of the Earth Observing One (EO-1) Mission, *IEEE Trans. Geosci. Remote Sens.*, 41(6 Part 1), 1149-1159.

WIEMKER, R., ROHR, K., BINDER, L., SPRENGEL, R. & STIEHL, H.S. (1996): Application of elastic registration to imagery from airborne scanners, *in* Proceedings of the International Archives for Photogrammetry and Remote Sensing, Vol 31, Part B, Commision IV, 6 pp.

WOODCOCK, C.E. & STRAHLER, A.H. (1987): The factor scale in remote sensing, *Remote Sens. Environ.*, 21, 311-332.

WOYCHEESE, J.P., PAGNI, P.J. & LIEPMANN, D. (1997): Brand lofting above large-scale fires, *in* Proceedings of the 2nd International Conference on Fire Research and Engineering (ICFRE2), August 3-8, 1997, Gaithersburg, MD, 137-150.